**Memo version 0.5**

# CEPC Analysis Memo

**March 31, 2020**

# Higgs boson decaying to ZZ* channel at the CEPC

Yanxi Gu[a], Min Zhong[a], Lingteng Kong[b], Ryuta Kiuchi[b], Xin Shi[b], Shih-Chieh Hsu[c], and Xinchou Lou[b]

[a]*Department of Modern Physics, University of Science and Technology of China, Hefei, China*
[b]*Institute of High Energy Physics, Beijing 100049, People's Republic of China*
[c]*Department of Physics, University of Washington, Seattle 98195-1560, USA*

## Abstract

# Contents

# ChangeLog

## version 0.6

- Change some plot size etc. to make the pdf file after compiling in good order
- Update fitting results (both cut-based and BDT) for 5 channels
- Fill the structure with plots/tables for each channel ( "$\mu\mu$", "$\nu\nu$", "$qq$" channels )

## version 0.5

- Update(add) author information
- Change the section numbering so as to start it from the introduction.
- Update the references which was not working, in the introduction section
- Add "Analysis Procedure" section. Add general desription about our analysis framework.
- Make a structure for each channel ( "$\mu\mu$", "$\nu\nu$", "$qq$" channels )

## Version 0.4

- Display the result of hvvjj channel

### Version 0.4.1

- Add pictures of signal's cut conditions

### Version 0.4.2

- Add background distribution

### Version 0.4.2

- change samples and update pictures and cut flow table

### Version 0.4.3

- 3/19/2019: 1.Update sample table, cut flow table and histograms, now the background in histograms are 2f, 4f and ZH. 2.Add present state of hjjvv channel.

### Version 0.4.4

- 4/25/2019: 1.Update results. 2. add equations for calculation

**Version 0.1.0**

- 5/10/2019: 1.Add introduction. 2. Add more for calculation part

# 1 Introduction

The historic discovery of a Higgs boson in 2012 by the ATLAS and CMS collaborations [1, 2] at the Large Hadron Collider (LHC) has opened a new era in particle physics. Subsequent measurements of the properties of the new particle have indicated compatibility with the Standard Model (SM) Higgs boson [3, 4, 5, 6, 7, 8, 9]. While the SM has been remarkably successful in describing experimental phenomena, it is important to recognize that it is not a complete theory. In particular, it does not *predict* the parameters in the Higgs potential, such as the Higgs boson mass. The vast difference between the Planck scale and the weak scale remains a major mystery. There is not a complete understanding of the nature of electroweak phase transition. The discovery of a spin zero Higgs boson, the first elementary particle of its kind, only sharpens these questions. It is clear that any attempt of addressing these questions will involve new physics beyond the SM (BSM). Therefore, the Higgs boson discovery marks the beginning of a new era of theoretical and experimental explorations.

A physics program of the precision measurements of the Higgs boson properties will be a critical component of any road map for high energy physics in the coming decades. Potential new physics beyond the SM could lead to observable deviations in the Higgs boson couplings from the SM expectations. Typically, such deviations can be parametrized as

$$\delta = c\frac{v^2}{M_{\mathrm{NP}}^2}, \tag{1}$$

where $v$ and $M_{\mathrm{NP}}$ are the vacuum expectation value of the Higgs field and the typical mass scale of new physics, respectively. The size of the proportionality constant $c$ depends on the model, but it should not be much larger than $O(1)$. The high-luminosity LHC (HL-LHC) will measure the Higgs boson couplings to about 5% [10, 11]. At the same time, the LHC will directly search for new physics from a few hundreds of GeV to at least one TeV. Eq. 1 implies that probing new physics significantly beyond the LHC reach would require the measurements of the Higgs boson couplings at least at percent level accuracy. To achieve such precision will need new facilities, a lepton collider operating as a Higgs factory is a natural next step.

The Circular Electron-Positron Collider CEPC, proposed by the Chinese particle physics community, is one of such possible facilities. The CEPC will be placed in a tunnel with a circumference of approximately 100 km and will operate at a center-of-mass energy of $\sqrt{s} \sim 240$ GeV, near the maximum of the Higgs boson production cross section through the $e^+e^- \to ZH$ process. At the CEPC, in contrast to the LHC, Higgs boson candidates can be identified through a technique known as the recoil mass method without tagging its decays. Therefore, the Higgs boson production can be disentangled from its decay in a model independent way. Moreover, the cleaner environment at a lepton collider allows much better exclusive measurements of Higgs boson decay channels. All of these give the CEPC an impressive reach in probing Higgs boson properties. With the expected integrated luminosity of $5.6 fb^{-1}$, over one million Higgs bosons will be produced. With this sample, the CEPC will be able to measure the Higgs boson coupling to the $Z$ boson with an accuracy of 0.25%, more than a factor of 10 better than the LHC. Such a precise measurement gives the CEPC unprecedented reach into interesting new physics scenarios which are difficult to probe at the LHC. The CEPC also has strong capability in detecting Higgs boson invisible decay. It is sensitive to the invisible decay branching ratio down to 0.3%. In addition, it is expected to have good sensitivities to exotic decay channels which are swamped by backgrounds at the LHC. It is also important to stress that an $e^+e^-$ Higgs factory can perform model independent measurement of the Higgs boson width. This unique feature in turn allows for the model independent determination of the Higgs boson couplings.

P.S. Above description given by Lineteng is almost the same as the first section of the CEPC white paper.(2019-12-08)

# 2 Samples

The analysis is performed on MC samples simulated on the CEPC conceptual detector. Sample path: $/cefs/data/DstData/CEPC240/CEPC\_v4/$, the details of samples is listed below, and the events expected is $5600fb^{-1}$

Table 1: The alias for particles

| | | |
|---|---|---|
| $uq : u, \bar{u}$ | $up : u, \bar{u}, c, \bar{c}$ | $nu_e : \nu_e, \overline{\nu}_e$ |
| $dq : d, \bar{d}$ | $down : d, \bar{d}, s, \bar{s}, b, \bar{b}$ | $nu_\mu : \nu_\mu, \overline{\nu}_\mu$ |
| $cq : c, \bar{c}$ | $e : e^-, e^+$ | $nu_\tau : \nu_\tau, \overline{\nu}_\tau$ |
| $sq : s, \bar{s}$ | $mu : \mu^-, \mu^+$ | $nu_{\mu,\tau} : \nu_{\mu,\tau}, \overline{\nu}_{\mu,\tau}$ |
| $bq : b, \bar{b}$ | $tau : \tau^-, \tau^+$ | $nu : \nu_{e,\mu,\tau}, \overline{\nu}_{e,\mu,\tau}$ |
| $f : e^-, \mu, \tau, \nu_e, \nu_\mu, \nu_\tau, u, d, c, s, b$ | | q:u,d,c,s,b |

## 2.1 ZH Samples

Table 2: ZH sample list

| Process | Cross section | Events expected |
|---|---|---|
| e1e1h_aa | 0.0161 | 90.24855 |
| e1e1h_az | 0.0108 | 60.5394 |
| e1e1h_bb | 4.06 | 22758.33 |
| e1e1h_cc | 0.205 | 1149.1275 |
| e1e1h_e2e2 | 0.00154 | 8.63247 |
| e1e1h_e3e3 | 0.445 | 2494.4475 |
| e1e1h_gg | 0.603 | 3380.1165 |
| e1e1h_ss | 0.0 | 0.0 |
| e1e1h_ww | 1.51 | 8464.305 |
| e1e1h_zz | 0.186 | 1042.623 |
| e2e2h_aa | 0.0154 | 86.3247 |
| e2e2h_az | 0.0104 | 58.2972 |
| e2e2h_bb | 3.91 | 21917.505 |
| e2e2h_cc | 0.197 | 1104.2835 |
| e2e2h_e2e2 | 0.00148 | 8.29614 |
| e2e2h_e3e3 | 0.428 | 2399.154 |
| e2e2h_gg | 0.58 | 3251.19 |
| e2e2h_ss | 0.0 | 0.0 |
| e2e2h_ww | 1.46 | 8184.03 |
| e2e2h_zz | 0.179 | 1003.3845 |
| e3e3h_aa | 0.0154 | 86.3247 |
| e3e3h_az | 0.0103 | 57.73665 |
| e3e3h_bb | 3.89 | 21805.395 |
| e3e3h_cc | 0.196 | 1098.678 |
| e3e3h_e2e2 | 0.00148 | 8.29614 |
| e3e3h_e3e3 | 0.427 | 2393.5485 |
| e3e3h_gg | 0.578 | 3239.979 |
| e3e3h_ss | 0.0 | 0.0 |
| e3e3h_ww | 1.45 | 8127.975 |
| e3e3h_zz | 0.178 | 997.779 |
| nnh_aa | 0.106 | 594.183 |
| nnh_az | 0.0708 | 396.8694 |
| nnh_bb | 26.7 | 149666.85 |
| nnh_cc | 1.35 | 7567.425 |
| nnh_e2e2 | 0.0101 | 56.61555 |
| nnh_e3e3 | 2.93 | 16424.115 |
| nnh_gg | 3.97 | 22253.835 |
| nnh_ss | 0.0 | 0.0 |
| nnh_ww | 9.95 | 55774.725 |
| nnh_zz | 1.22 | 6838.71 |
| qqh_aa | 0.312 | 1748.916 |
| qqh_az | 0.209 | 1171.5495 |
| qqh_bb | 78.9 | 442273.95 |
| qqh_cc | 3.98 | 22309.89 |
| qqh_e2e2 | 0.03 | 168.165 |
| qqh_e3e3 | 8.65 | 48487.575 |
| qqh_gg | 11.7 | 65584.35 |
| qqh_ss | 0.0 | 0.0 |
| qqh_ww | 29.4 | 164801.7 |
| qqh_zz | 3.61 | 20235.855 |

## 2.2 Two fermions background Samples

Table 3: General information about two fermions background samples

| Process | Cross section | Events expected |
|---|---|---|
| qq | 54106.86 | 303296003.73 |
| e2e2 | 5332.71 | 29892506.46 |
| e3e3 | 4752.89 | 26642325.45 |
| e1e1 | 24770.9 | 138853279.95 |
| n1n1 | 45390.79 | 254438073.9 |
| n2n2 | 4416.3 | 24755569.65 |
| n3n3 | 4410.26 | 24721712.43 |

## 2.3 Four fermions background Samples

Table 4: General information about four fermions background samples

| Process | Cross section | Events expected |
|---|---|---|
| zz_h0utut | 85.68 | 480279.24 |
| zz_h0dtdt | 233.46 | 1308660.03 |
| zz_h0uu_notd | 98.56 | 552478.08 |
| zz_h0cc_nots | 98.97 | 554776.89 |
| zz_sl0nu_up | 84.38 | 472992.09 |
| zz_sl0nu_down | 139.71 | 783144.96 |
| zz_sl0mu_up | 87.39 | 489865.2 |
| zz_sl0mu_down | 136.14 | 763132.77 |
| zz_sl0tau_up | 41.56 | 232964.58 |
| zz_sl0tau_down | 67.31 | 377306.76 |
| zz_l04tau | 4.61 | 25841.91 |
| zz_l04mu | 15.56 | 87221.58 |
| zz_l0taumu | 18.56 | 104038.08 |
| zz_l0mumu | 19.38 | 108634.59 |
| zz_l0tautau | 9.61 | 53869.41 |
| ww_h0cuxx | 3478.89 | 19500918.45 |
| ww_h0uubd | 0.05 | 280.83 |
| ww_h0uusd | 170.45 | 955458.03 |
| ww_h0ccbs | 5.89 | 33016.95 |
| ww_h0ccds | 170.18 | 953943.99 |
| ww_sl0muq | 2423.43 | 13584537.42 |
| ww_sl0tauq | 2423.56 | 13585265.58 |
| ww_l0ll | 403.66 | 2262716.13 |
| zzorww_h0udud | 1610.32 | 9026648.76 |
| zzorww_h0cscs | 1607.55 | 9011122.08 |
| zzorww_l0mumu | 221.1 | 1239376.05 |
| zzorww_l0tautau | 211.18 | 1183769.49 |
| sze_l0tau | 147.28 | 825578.04 |
| sze_l0mu | 845.81 | 4741188.51 |
| sze_l0nunu | 28.94 | 162223.17 |
| sze_sl0uu | 190.21 | 1066222.71 |
| sze_sl0dd | 125.83 | 705340.62 |
| sznu_l0mumu | 43.42 | 243390.81 |
| sznu_l0tautau | 14.57 | 81672.69 |
| sznu_sl0nu_up | 55.59 | 311610.3 |
| sznu_sl0nu_down | 90.03 | 504663.72 |
| sw_l0mu | 436.7 | 2447921.85 |
| sw_l0tau | 435.93 | 2443606.17 |
| sw_sl0qq | 2612.62 | 14645041.41 |
| szeorsw_l0l | 249.48 | 1398460.14 |

# 3 Analysis Procedure

We give here a brief explanation about the analysis framework which is common to all of indivisual channels. The Marlin framework is used for this flow.

The analysis starts from the reconstructed objects as inputs. The lepton isolation processor, the jet clustering processor are applied on the Arbor PFO to separate leptons from the rest. The remain objects are going to be clustered into number of jets by the the jet clustering processor, where we can designate the jet algorithm to be used, the number of (exclusive) jets and so on. Classified objects are feed into a processor which we call it internally as “Higgs2zz” processor and pre selection on events are performed. Fig. 1 is the skematic of the analysis flow chart, and further details are given in the following items.

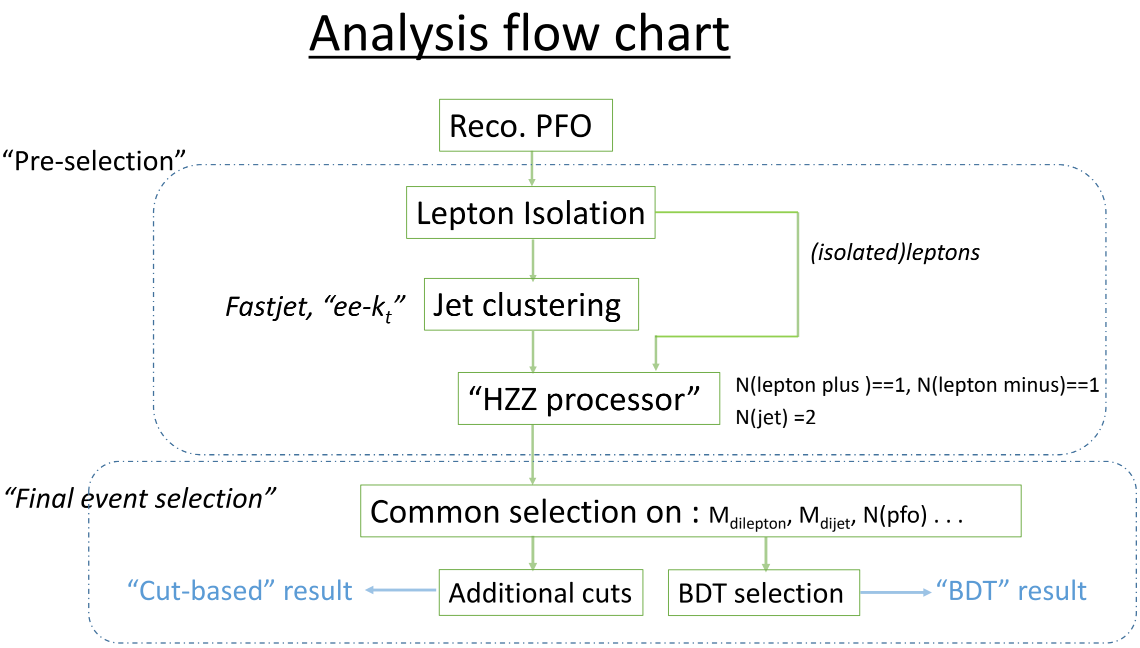


Figure 1: Analysis Flow Chart

Lepton Isolation

The leptons, here they are electrons and muons, like the decay particles of the initial Z boson, should not be merged into jets, and the task is done by this lepton isoloation processor. The isolated status is judged from several condistions, such as particles having “cone energy” which is lower than certain thredhold, as well as requiring its PID as that of electrons or muons. The input collection to the processor is the Arbor PFO, and it has two output collections, one includes only isolated leptons, the other includes the rest.

### Jet Clustering

FastJet processor has been chosen for the jet clustering process. We have used so-called "ee-kt" algorithm. The input collection is the one which does not include isolated leptons, and that is clustered into two jets exclusively, by setting the number of jets option as two. The output collection of this processor has information of these two jets.

### Event Preselection

The "Higgs2zz" processor has role of the event preselection. The input collections consists of output of the lepton isolation processor for the isolated leptons, output of the fastjet processor for the jets, the Arbor PFO collection and the MCParticle collection for MC truth information. If event contains one positive charged lepton and one minus charged lepton in the isolated lepton collection, and the two jets from the fastjet processor, this event is saved. Several meaningful information, such as di lepton mass and momentum, are obtained at this stage and as well.

Typical distributions after this pre selection process on $\mu\mu$HZZ signal sample are shown in Fig. 2-3. Corresponding description about the histograms should be given briefly here.

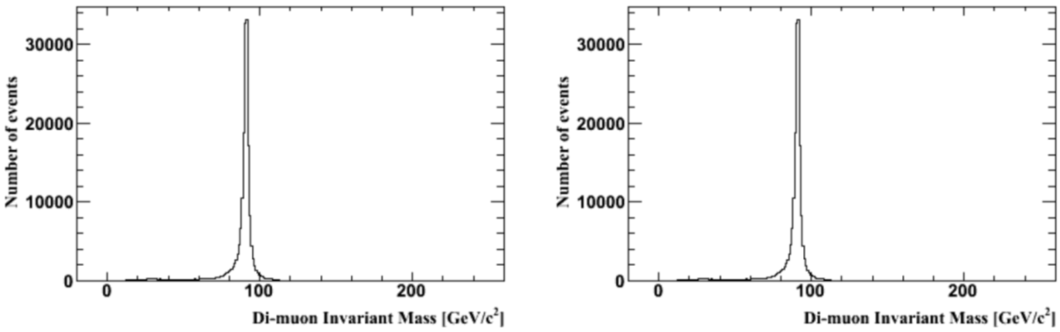


Figure 2: Distributions of the invariant mass and the recoil mass of di-muons. The figures shall be updated. .

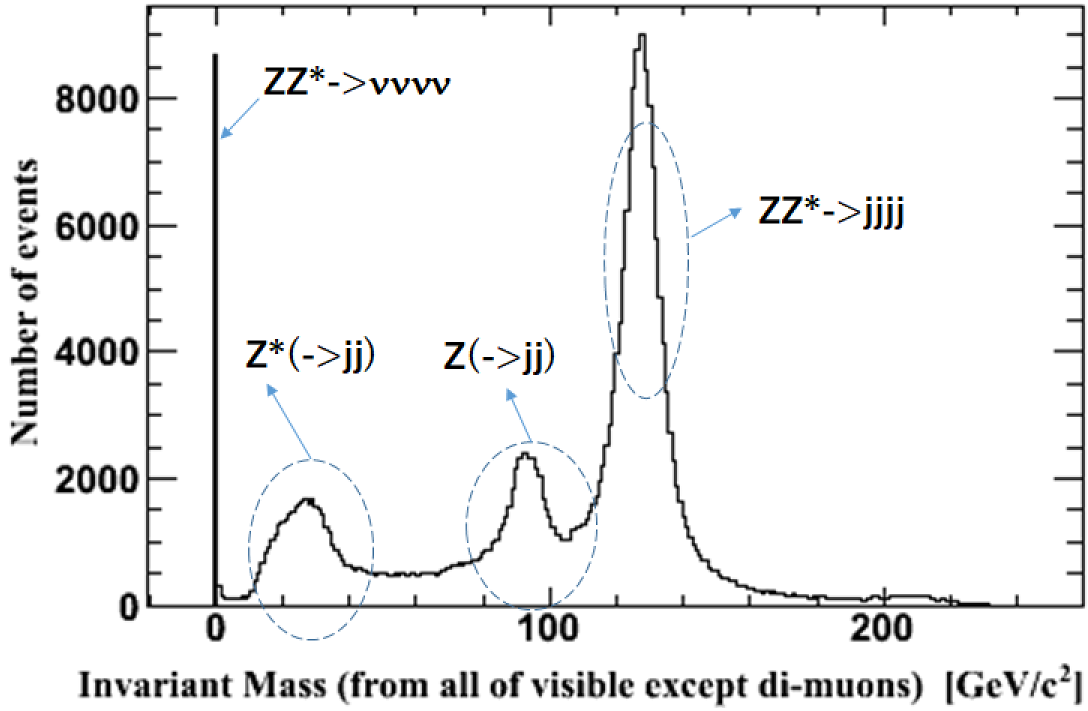


Figure 3: Visible (but except the di-muons) mass distribution. Or, di-jet invariant mass distribution.. The figures shall be updated. .

# 4 Event Selection of Z(→$\mu\mu$)H(ZZ*→$\nu\nu qq$)

## 4.1 Z(→ $\mu^+\mu^-$), H(Z→$\nu\bar{\nu}$, Z*→$q\bar{q}$)

### 4.1.1 Event selection (Cut-based only)

Table 5: Cut flow table for $\mu\mu\nu\nu qq$ channel

| Cut | Signal | ZH background | 2f background | 4f background | $\frac{S}{\sqrt{S+B}}$ |
|---|---|---|---|---|---|
| $Expected$ | 1000 | 1140511 | 801811977 | 107203890 | |
| $Pre-selection$ | 616 | 30494 | 480828 | 515448 | |
| $Signal\ or\ not$ | 211 | 30282 | 480828 | 515448 | |
| $M_{missing} > M_{dijet}$ | 107 | 1608 | 115062 | 28809 | 0.283 |
| $N(pfo)$ | 104 | 908 | 33480 | 14159 | 0.4722 |
| $M_{dimuon}$ | 92 | 296 | 24151 | 1625 | 0.5714 |
| $M_{dijet}$ | 87 | 280 | 851 | 819 | 1.9395 |
| $M_{missing}$ | 71 | 124 | 97 | 101 | 3.6196 |
| $cos\theta_{visible}$ | 68 | 118 | 22 | 39 | 4.349 |
| $Angle_{\mu j}$ | 62 | 95 | 14 | 20 | 4.4919 |
| $M^{rec}_{dimuon}$ | 61 | 79 | 14 | 8 | 4.7795 |
| $M^{rec}_{dijet}$ | 59 | 69 | 0 | 4 | 5.1374 |
| $not\ qqHZZ$ | 59 | 69 | 0 | 4 | 5.1374 |
| $not\ \nu\nu HZZ$ | 50 | 36 | 0 | 4 | 5.2503 |

Table 6: Remained backgrounds (more than 1 event) after all of cuts applied.

| name | scale | final |
|---|---|---|
| e2e2h_e3e3 | 0.023968 | 2 |
| e2e2h_ww | 0.08176 | 22 |
| nnh_zz | 0.06832 | 10 |
| zz_sl0mu_down | 1.08025726079 | 1 |
| zz_sl0tau_up | 1.10880522921 | 1 |
| zz_l0taumu | 1.0404004004 | 2 |

The event selection cuts are listed below in sequence.

- $M_{miss} > M_{dijets}$ : the missing mass is greater than the dijet invariant mass.

- $20 < N_{pfo} < 90$ : Number of Prticle Flow Objects should be in this range.

- $80GeV < M_{\mu^+\mu^-} < 100GeV$ : the invariant mass of the dimuon should be in this range.

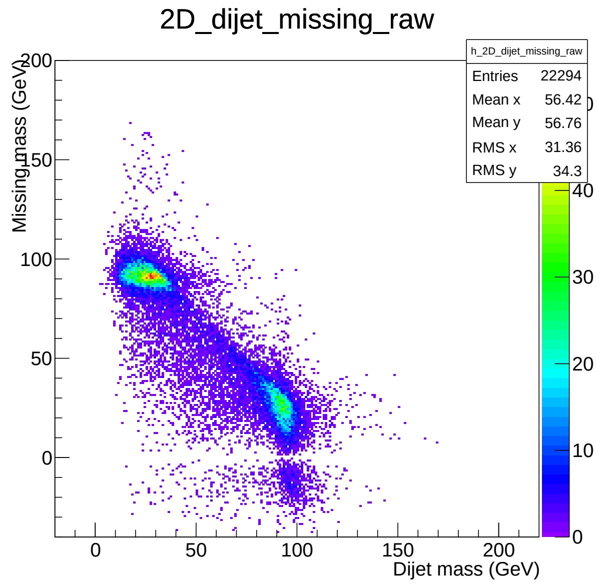


Figure 4: Missing mass vs dijet invariant mass.

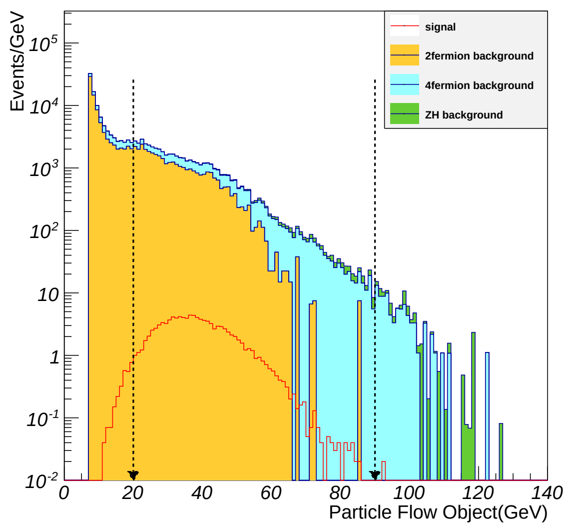


Figure 5: Number of PFOs.

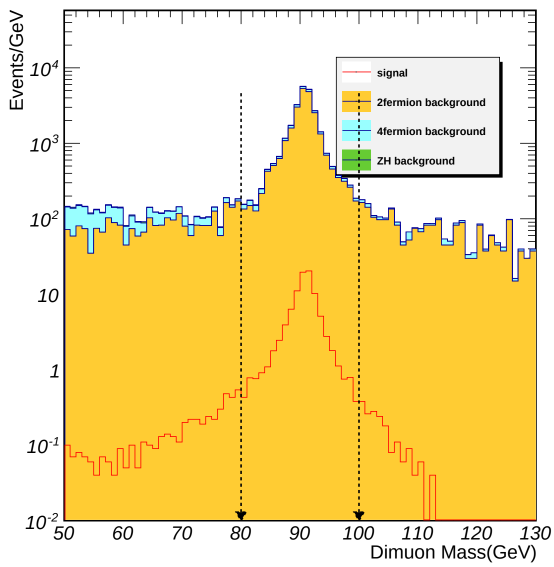


Figure 6: Invariant mass of di-muons.

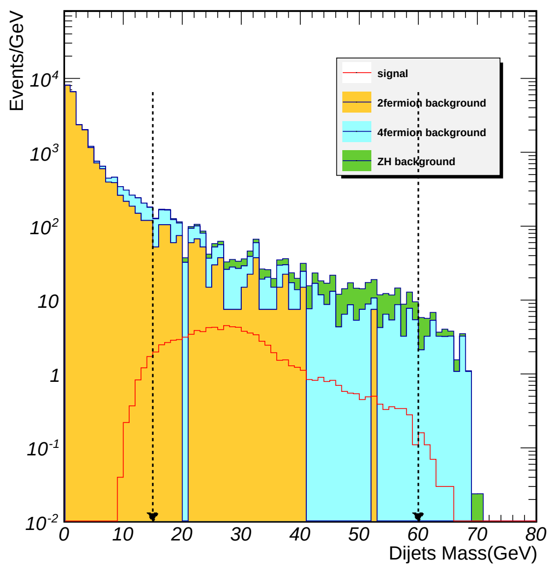


Figure 7: Invariant mass of di-jets.

- $15GeV < M_{dijet} < 60GeV$ : the invariant mass of dijet should be in this range.

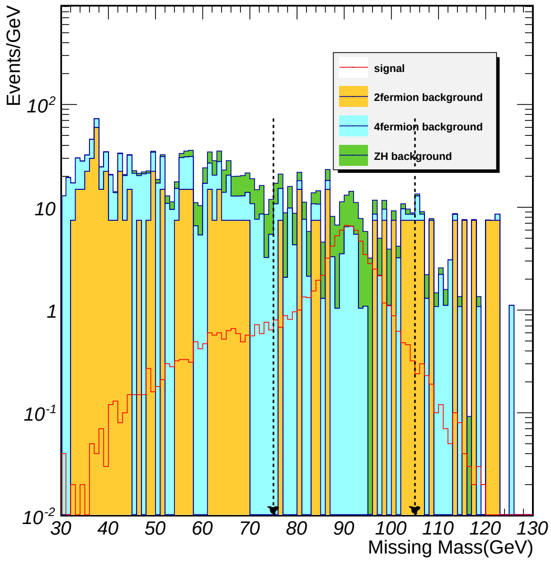


Figure 8: Recoil mass of visible particles.

- $75GeV < M^{Recoil}_{visible} < 105GeV$ : the recoil mass of all visible particles should be in this range.

- $-0.95 < cos_{plain} < 0.95$ : Cos calculated by all visible particle Pz and Py should be in this range

- $60 < Min\ angle < 170°$: Minimum angle between the two Z(Z*) reconstructed by leptons and jets should be within this range .

- $110GeV < M^{dimuon}_{Recoil} < 140GeV$: the recoil mass of the dimuon should be in this range.

- $185GeV < M^{dijet}_{Recoil} < 220GeV$: the recoil mass of the dijet should be in this range.

Two additional cuts:

- $M^{rec}_{dijet} < 122GeV\ or\ M^{rec}_{dijet} > 128GeV$ : To avoid the overlap events with $qq$HZZ signals.
- $M_{visible} < 122GeV\ or\ M_{visible} > 128GeV$ : To remove the overlap events with $\nu\nu$HZZ signals.

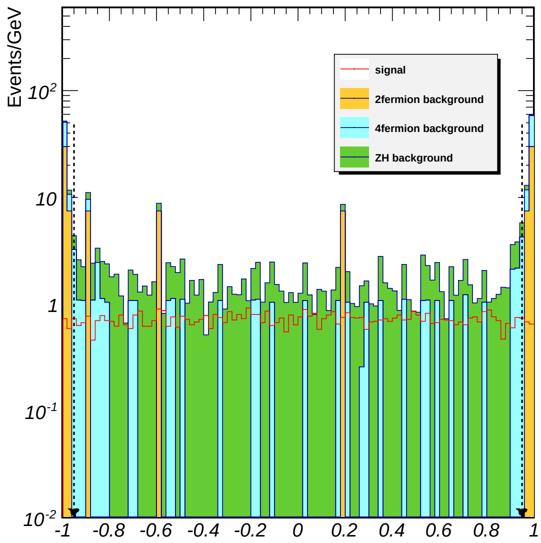


Figure 9: All visible particle *cos θ*

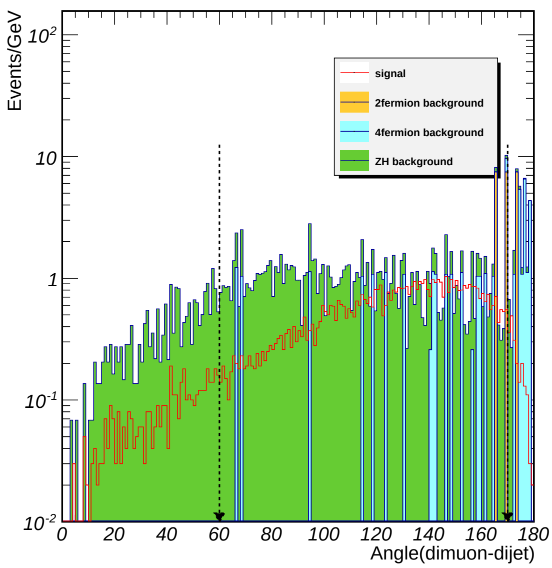


Figure 10: Minimum angle between the two Z(Z*) reconstructed by leptons and jets.

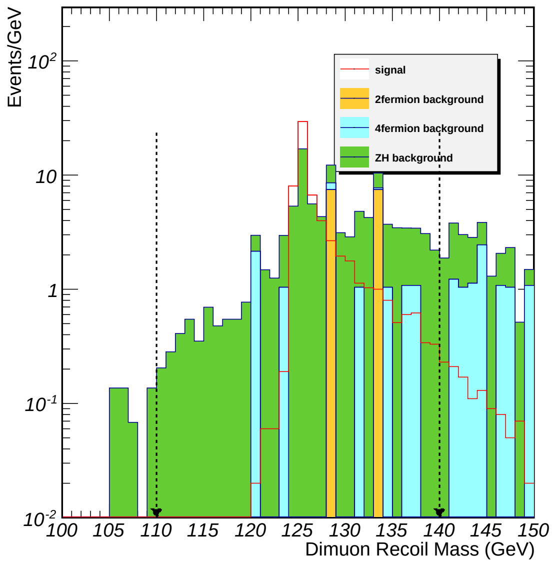


Figure 11: Recoil mass of di-muons.

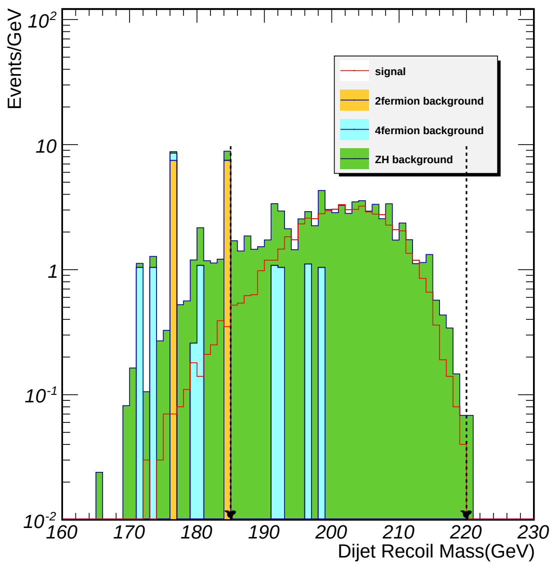


Figure 12: Recoil mass of di-jets.

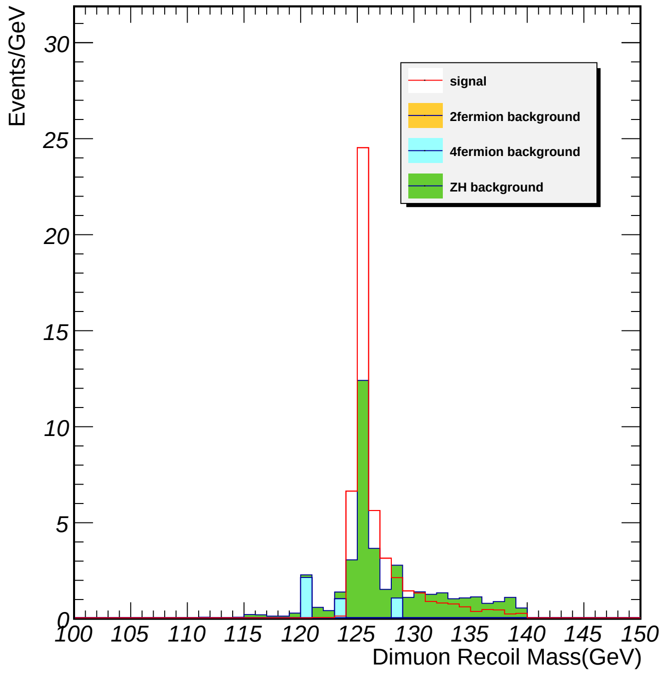


Figure 13: Distribution of the recoil mass of dimuon, after all of cuts applied.

## 4.2 Z($\rightarrow \mu^+\mu^-$), H(Z$\rightarrow q\bar{q}$, Z*$\rightarrow \nu\bar{\nu}$)

### 4.2.1 Event selection (Cut-based only)

The event selection cuts are listed below in sequence.

- $M_{miss} > M_{dijets}$ : the missing mass is greater than the dijet invariant mass.
- $30 < N_{pfo} < 100$ : Number of Prticle Flow Objects should be in this range.
- $80GeV < M_{\mu^+\mu^-} < 100GeV$ : the invariant mass of the dimuon should be in this range.
- $60GeV < M_{dijet} < 105GeV$ : the invariant mass of dijet should be in this range.
- $10GeV < M^{Recoil}_{visible} < 55GeV$ : the recoil mass of all visible particles should be in this range.
- $-0.95 < cos_{plain} < 0.95$ : Cos calculated by all visible particle Pz and Py should be in this range

Table 7: Cut flow table for $\mu\mu qq\nu\nu$ channel

| Cut | Signal | ZH background | 2f background | 4f background | $\frac{S}{\sqrt{S+B}}$ |
|---|---|---|---|---|---|
| $Expected$ | 1000 | 1140511 | 801811977 | 107203890 | |
| $Pre-selection$ | 616 | 30494 | 480828 | 515448 | |
| $Signal\ or\ not$ | 211 | 30282 | 480828 | 515448 | |
| $M_{missing} < M_{dijet}$ | 103 | 28674 | 365766 | 486638 | 0.1102 |
| $N(pfo)$ | 100 | 21686 | 12184 | 332162 | 0.1657 |
| $M_{dimuon}$ | 89 | 16833 | 9085 | 207927 | 0.186 |
| $M_{dijet}$ | 82 | 2768 | 52 | 173775 | 0.1974 |
| $M_{missing}$ | 71 | 1679 | 14 | 13434 | 0.5804 |
| $*cos\ \theta$ | 71 | 1679 | 14 | 13434 | 0.5804 |
| $cos\theta_{visible}$ | 67 | 1535 | 0 | 8545 | 0.6749 |
| $Angle_{\mu j}$ | 57 | 1109 | 0 | 2197 | 0.995 |
| $M^{rec}_{dimuon}$ | 56 | 1048 | 0 | 941 | 1.2488 |
| $*M^{rec}_{dijet}$ | 56 | 1048 | 0 | 941 | 1.2488 |
| $M_{visible}$ | 54 | 930 | 0 | 790 | 1.2823 |
| $*P_{visible}$ | 54 | 930 | 0 | 790 | 1.2823 |
| $*P_{T_{visible}}$ | 54 | 930 | 0 | 790 | 1.2823 |
| $*E_{leading\ jet}$ | 54 | 930 | 0 | 790 | 1.2823 |
| $*P_{T_{leading\ jet}}$ | 54 | 930 | 0 | 790 | 1.2823 |
| $*E_{sub-leading\ jet}$ | 54 | 930 | 0 | 790 | 1.2823 |
| $*P_{T_{sub-leading\ jet}}$ | 54 | 930 | 0 | 790 | 1.2823 |
| $not\ qqHZZ$ | 46 | 738 | 0 | 644 | 1.2343 |
| $not\ \nu\nu HZZ$ | 46 | 738 | 0 | 644 | 1.2343 |

Table 8: Remained backgrounds (more than 1 event) after all of cuts applied.

| name | scale | final |
|---|---|---|
| e2e2h_bb | 0.21896 | 405 |
| e2e2h_cc | 0.011032 | 5 |
| e2e2h_e3e3 | 0.023968 | 5 |
| e2e2h_gg | 0.0326888819557 | 1 |
| e2e2h_ww | 0.08176 | 282 |
| e2e2h_zz | 0.010024 | 6 |
| e3e3h_zz | 0.009968099681 | 1 |
| qqh_e3e3 | 0.4844 | 7 |
| qqh_ww | 1.6464 | 1 |
| qqh_zz | 0.20216 | 21 |
| zz_sl0mu_up | 1.09032214858 | 159 |
| zz_sl0mu_down | 1.08025726079 | 473 |
| zz_sl0tau_down | 1.10887174477 | 5 |
| ww_sl0muq | 1.2235862395 | 6 |

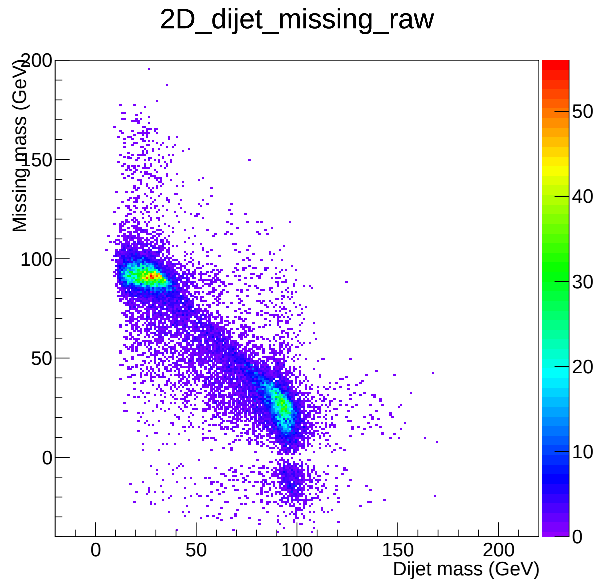


Figure 14: Missing mass vs dijet invariant mass.

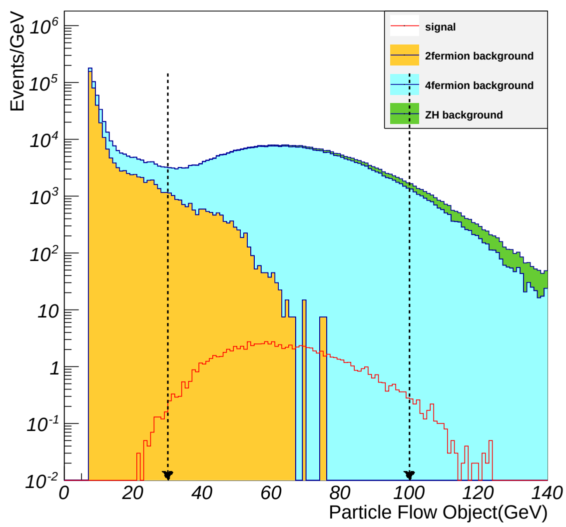


Figure 15: Number of PFOs.

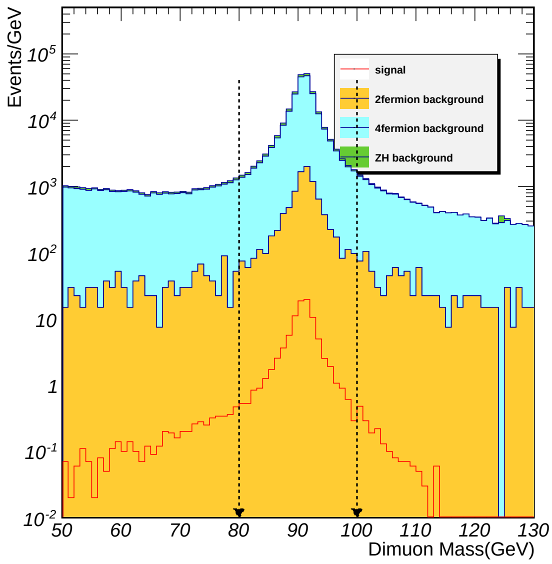


Figure 16: Invariant mass of di-muons.

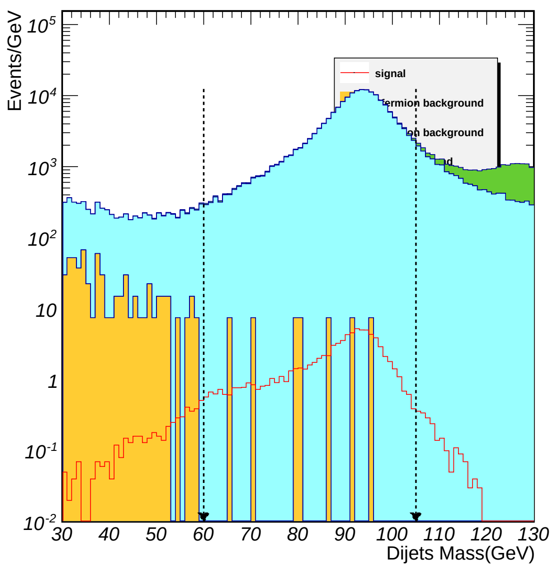


Figure 17: Invariant mass of di-jets.

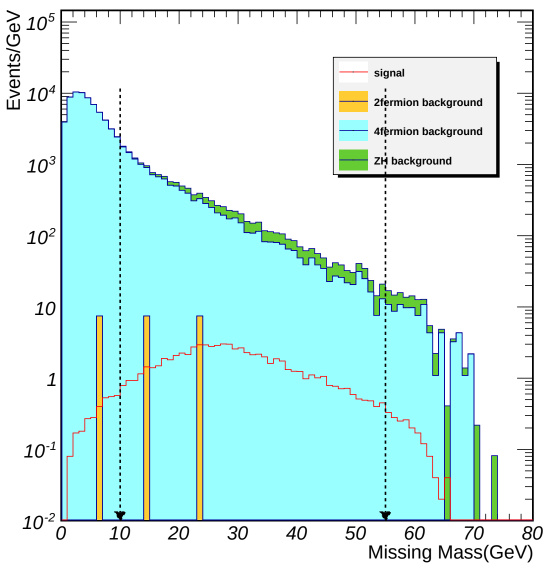


Figure 18: Recoil mass of visible particles.

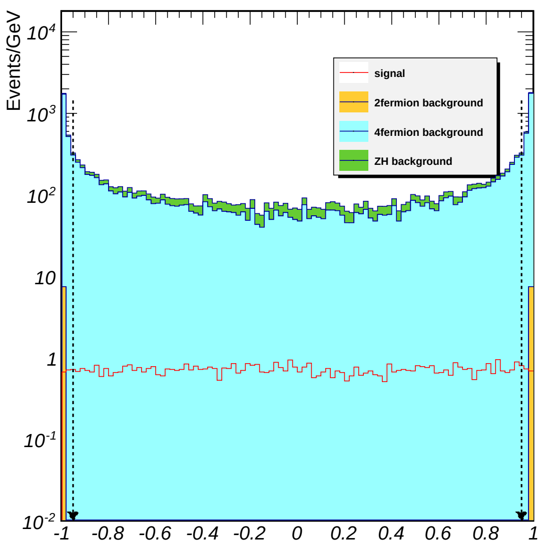


Figure 19: All visible particle $cos\ \theta$

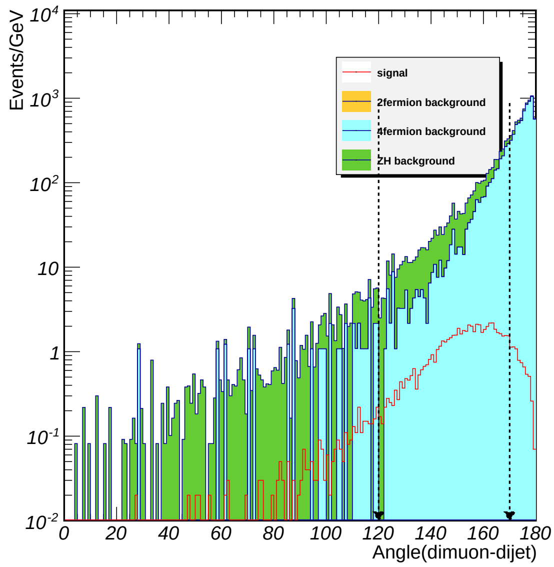


Figure 20: Minimum angle between the two Z(Z*) reconstructed by leptons and jets.

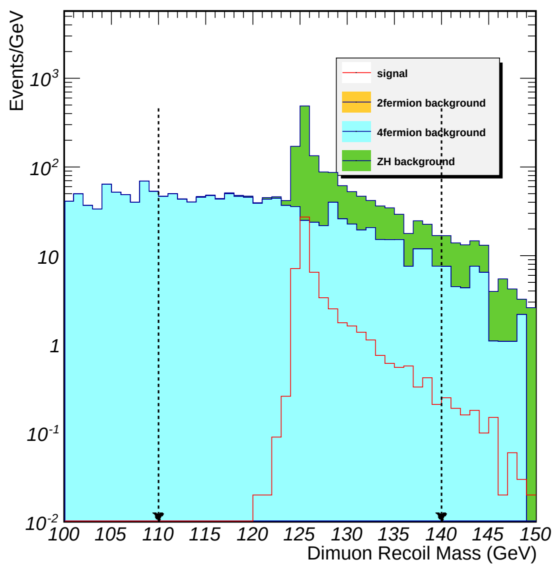


Figure 21: Recoil mass of di-muons.

- $120 < Min\ angle < 170°$: Minimum angle between the two Z(Z*) reconstructed by leptons and jets should be within this range .

- $110GeV < M^{dimuon}_{Recoil} < 140GeV$: the recoil mass of the dimuon should be in this range.

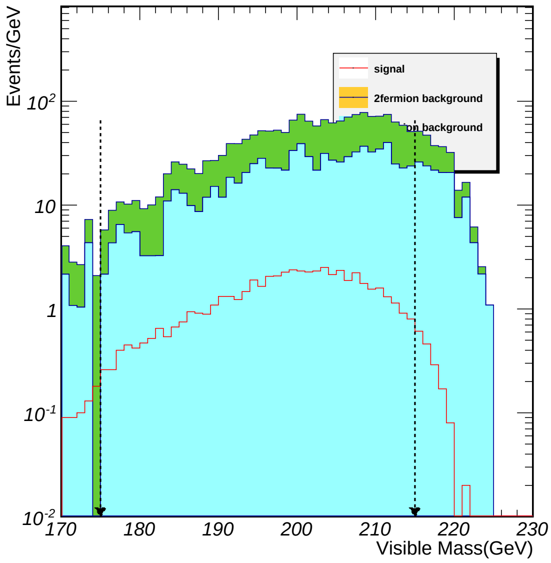


Figure 22: Visible mass of all particles.

- $175GeV < M_{visible} < 215GeV$: the visible mass of all particles should be in this range.

Two additional cuts:

- $M^{rec}_{dijet} < 122GeV\ or\ M^{rec}_{dijet} > 128GeV$ : To avoid the overlap events with $qq$HZZ signals.
- $M_{visible} < 122GeV\ or\ M_{visible} > 128GeV$ : To remove the overlap events with $\nu\nu$HZZ signals.

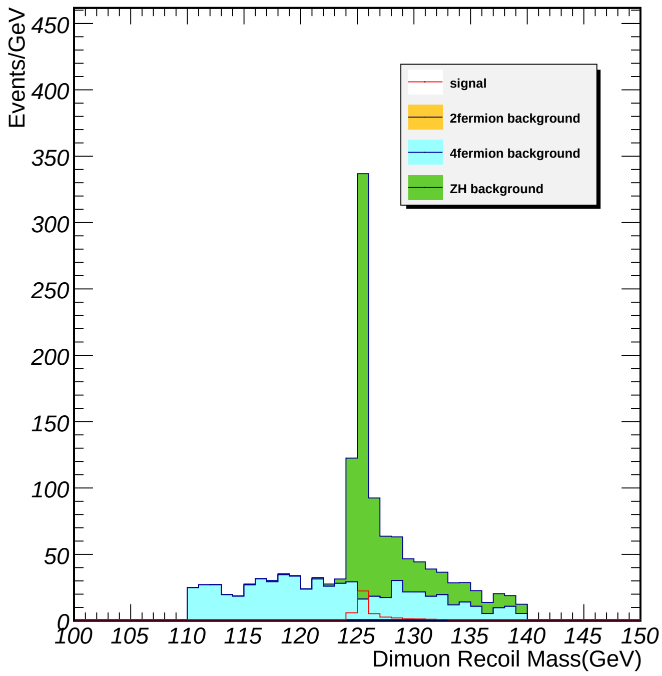


Figure 23: Distribution of the recoil mass of dimuon, after all of cuts applied.

# 5 Event Selection of Z(→$\nu\nu$)H(ZZ*→$\mu\mu qq$)

## 5.1 Z(→ $\nu\bar{\nu}$), H(ZZ*→$\mu^+\mu^-$→$q\bar{q}$)

### 5.1.1 Event selection (Cut-based only)

Table 9: Cut flow table for $\nu\nu\mu\mu qq$ channel

| Cut | Signal | ZH background | 2f background | 4f background | $\frac{S}{\sqrt{S+B}}$ |
|---|---|---|---|---|---|
| $Expected$ | 6844 | 1140511 | 801811977 | 107203890 | |
| $Pre-selection$ | 238 | 30494 | 480828 | 515424 | |
| $Signal\ or\ not$ | 226 | 30268 | 480828 | 515424 | |
| $M_{dimuon} > M_{dijet}$ | 125 | 2832 | 421952 | 156993 | 0.1642 |
| $N(pfo)$ | 117 | 1259 | 60398 | 68100 | 0.325 |
| $M_{missing}$ | 102 | 147 | 2152 | 791 | 1.8168 |
| $M_{dimuon}$ | 95 | 136 | 1762 | 258 | 2.007 |
| $M_{dijet}$ | 94 | 131 | 258 | 204 | 3.5888 |
| $*cos\ \theta$ | 94 | 131 | 258 | 204 | 3.5888 |
| $cos\theta_{visible}$ | 89 | 125 | 37 | 57 | 5.0842 |
| $Angle_{\mu j}$ | 83 | 72 | 0 | 16 | 6.3751 |
| $*M^{rec}_{dimuon}$ | 83 | 72 | 0 | 16 | 6.3751 |
| $*M^{rec}_{dijet}$ | 83 | 72 | 0 | 16 | 6.3751 |
| $M_{visible}$ | 83 | 56 | 0 | 11 | 6.7871 |
| $*P_{visible}$ | 83 | 56 | 0 | 11 | 6.7871 |
| $*P_{T_{visible}}$ | 83 | 56 | 0 | 11 | 6.7871 |
| $*E_{leading\ jet}$ | 83 | 56 | 0 | 11 | 6.7871 |
| $*P_{T_{leading\ jet}}$ | 83 | 56 | 0 | 11 | 6.7871 |
| $*E_{sub-leading\ jet}$ | 83 | 56 | 0 | 11 | 6.7871 |
| $*P_{T_{sub-leading\ jet}}$ | 83 | 56 | 0 | 11 | 6.7871 |
| $not\ \mu^+\mu^- HZZ$ | 72 | 17 | 0 | 9 | 7.2837 |
| $not\ qqHZZ$ | 72 | 17 | 0 | 9 | 7.2837 |

The event selection cuts are listed below in sequence.

- $M_{dimuon} > M_{dijets}$ : the dimuon invariant mass is greater than the dijet invariant mass.

- $20 < N_{pfo} < 60$ : Number of Prticle Flow Objects should be in this range.

- $75GeV < M^{Recoil}_{visible} < 110GeV$ : the recoil mass of all visible particles should be in this range.

- $60GeV < M_{\mu^+\mu^-} < 100GeV$ : the invariant mass of the dimuon should be in this range.

Table 10: Remained backgrounds (more than 1 event) after all of cuts applied.

| name | scale | final |
|---|---|---|
| e2e2h_ww | 0.08176 | 4 |
| e2e2h_zz | 0.010024 | 9 |
| e3e3h_ww | 0.0812 | 2 |
| zz_sl0tau_up | 1.10880522921 | 1 |
| zz_l0taumu | 1.0404004004 | 1 |
| ww_sl0muq | 1.10890944134 | 3 |
| ww_sl0tauq | 1.10899434445 | 1 |
| zzorww_l0mumu | 1.10891486372 | 1 |
| sze_l0mu | 1.10916641266 | 1 |

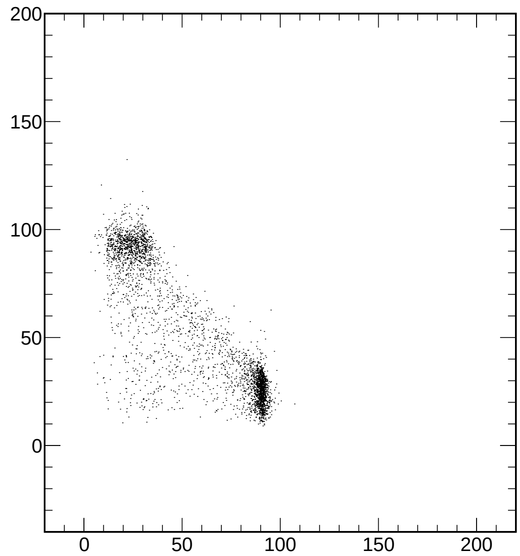


Figure 24: dimuon invariant mass vs dijet invariant mass.

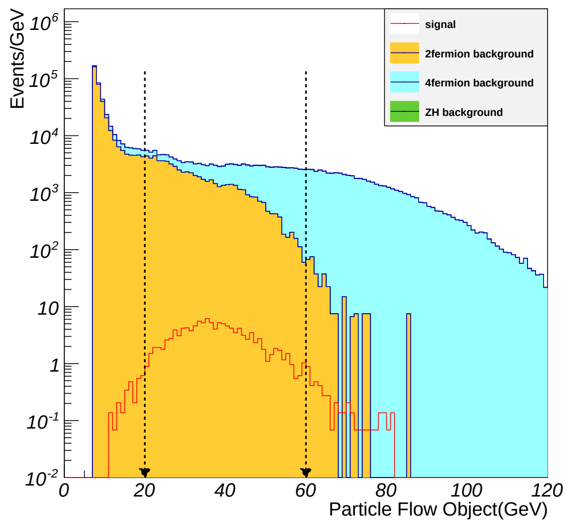


Figure 25: Number of PFOs.

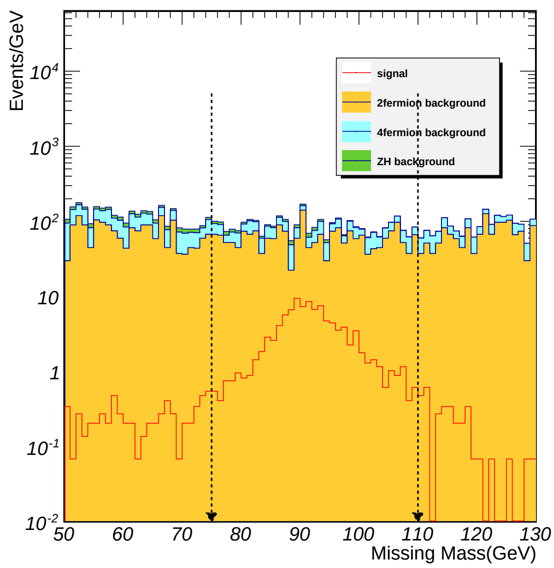


Figure 26: Recoil mass of visible particles.

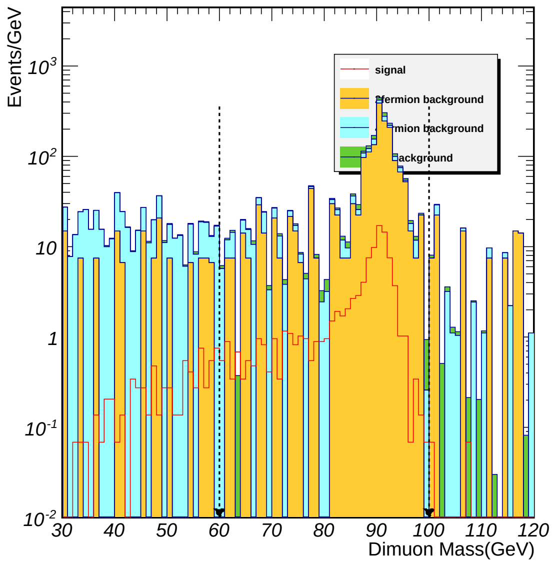


Figure 27: Invariant mass of di-muons.

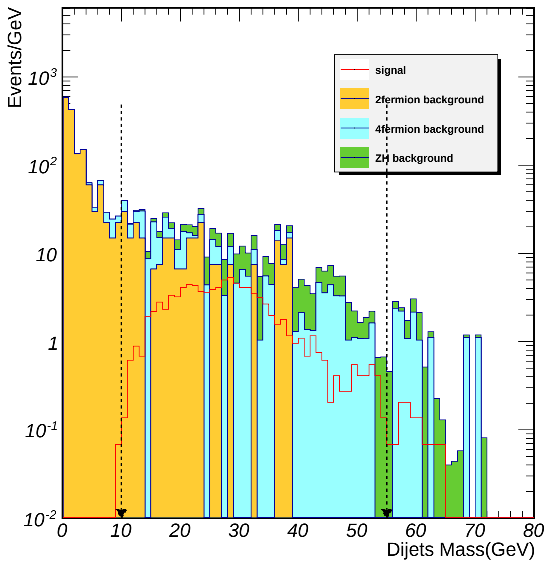


Figure 28: Invariant mass of di-jets.

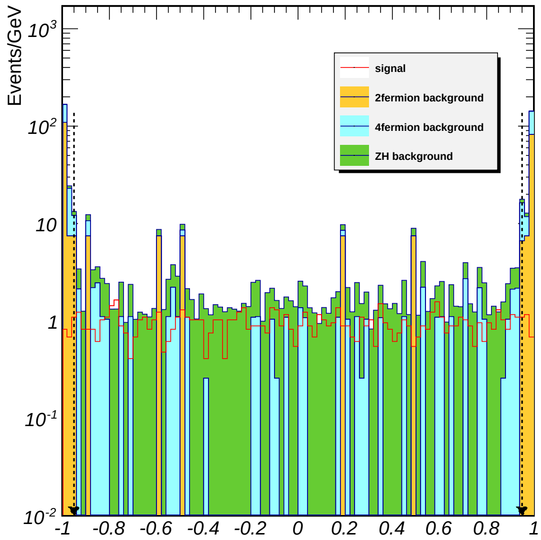


Figure 29: All visible particle $cos\ \theta$

- $10GeV < M_{dijet} < 55GeV$ : the invariant mass of dijet should be in this range.

- $-0.95 < cos_{plain} < 0.95$ : Cos calculated by all visible particle Pz and Py should be in this range

- $Min\ angle\ < 135°$: Minimum angle between the two Z(Z*) reconstructed by leptons and jets should be within this range .

- $110GeV < M_{visible} < 140GeV$ : the invariant mass of all visible particles should be in this range.

Two additional cuts:

- $M^{rec}_{dimuon} < 122GeV\ or\ M^{rec}_{dimuon} > 128GeV$ : To avoid the overlap events with $\mu\mu$HZZ signals.
- $M^{rec}_{dijet} < 122GeV\ or\ M^{rec}_{dijet} > 128GeV$ : To remove the overlap events with $qq$HZZ signals.

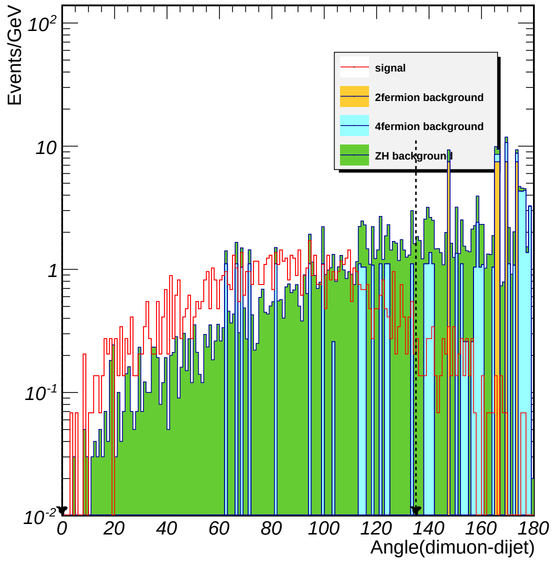


Figure 30: Minimum angle between the two Z(Z*) reconstructed by leptons and jets.

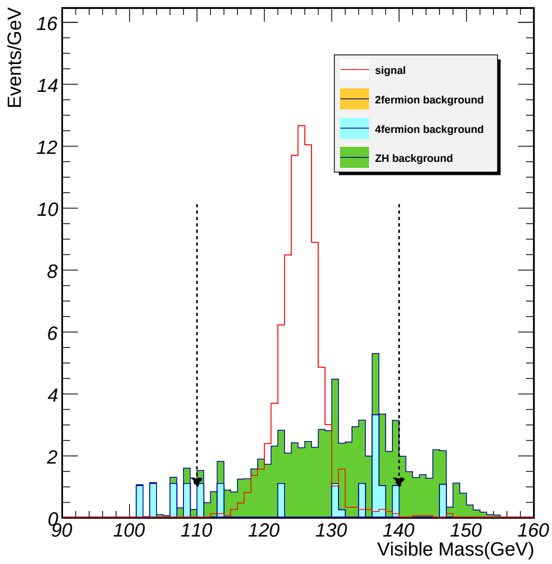


Figure 31: Invariant mass of all visible particles.

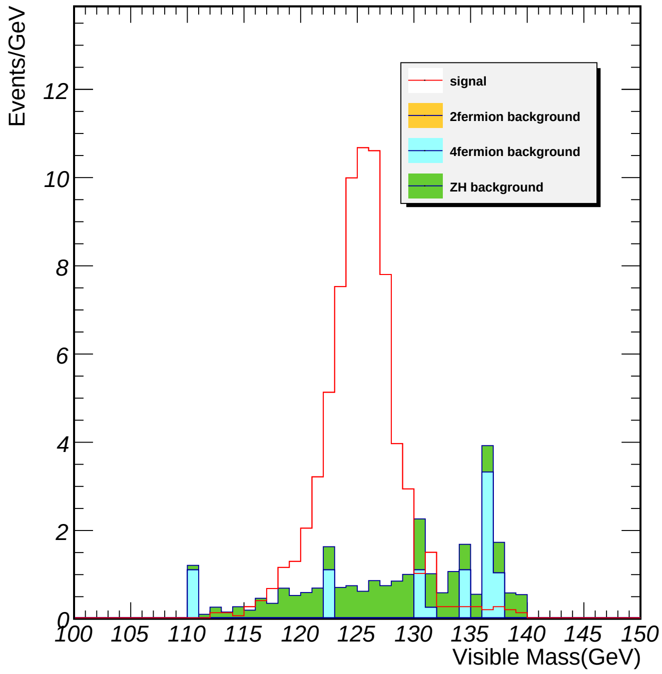


Figure 32: Distribution of the visible mass of all particles, after all of cuts applied.

## 5.2 Z($\rightarrow \nu\bar{\nu}$), H(Z$\rightarrow q\bar{q}$, Z*$\rightarrow\mu^{+}\mu^{-}$)

### 5.2.1 Event selection (Cut-based only)

The event selection cuts are listed below in sequence.

- $M_{dimuon} < M_{dijets}$ : the dijet invariant mass is greater than the dimuon invariant mass.
- $30 < N_{pfo} < 100$ : Number of Prticle Flow Objects should be in this range.
- $75GeV < M^{Recoil}_{visible} < 110GeV$ : the recoil mass of all visible particles should be in this range.
- $10GeV < M_{\mu^{+}\mu^{-}} < 60GeV$ : the invariant mass of the dimuon should be in this range.
- $60GeV < M_{dijet} < 100GeV$ : the invariant mass of dijet should be in this range.
- $-0.95 < cos_{plain} < 0.95$ : Cos calculated by all visible particle Pz and Py should be in this range

Table 11: Cut flow table for $\nu\nu qq\mu\mu$ channel

| Cut | Signal | ZH background | 2f background | 4f background | $\frac{S}{\sqrt{S+B}}$ |
|---|---|---|---|---|---|
| $Expected$ | 6844 | 1140511 | 801811977 | 107203890 | |
| $Pre-selection$ | 238 | 30494 | 480828 | 515424 | |
| $Signal\ or\ not$ | 226 | 30268 | 480828 | 515424 | |
| $M_{dimuon} < M_{dijet}$ | 101 | 27436 | 58876 | 358431 | 0.1521 |
| $N(pfo)$ | 97 | 20843 | 364 | 231698 | 0.1939 |
| $M_{missing}$ | 79 | 769 | 37 | 2083 | 1.4508 |
| $M_{dimuon}$ | 78 | 707 | 7 | 1732 | 1.5596 |
| $M_{dijet}$ | 68 | 576 | 0 | 830 | 1.7719 |
| $*cos\ \theta$ | 68 | 576 | 0 | 830 | 1.7719 |
| $cos\theta_{visible}$ | 64 | 552 | 0 | 452 | 1.9743 |
| $Angle_{\mu j}$ | 59 | 239 | 0 | 70 | 3.1041 |
| $M^{rec}_{dimuon}$ | 58 | 214 | 0 | 65 | 3.184 |
| $*M^{rec}_{dijet}$ | 58 | 214 | 0 | 65 | 3.184 |
| $M_{visible}$ | 57 | 175 | 0 | 54 | 3.4122 |
| $*P_{visible}$ | 57 | 175 | 0 | 54 | 3.4122 |
| $*P_{T_{visible}}$ | 57 | 175 | 0 | 54 | 3.4122 |
| $*E_{leading\ jet}$ | 57 | 175 | 0 | 54 | 3.4122 |
| $*P_{T_{leading\ jet}}$ | 57 | 175 | 0 | 54 | 3.4122 |
| $*E_{sub-leading\ jet}$ | 57 | 175 | 0 | 54 | 3.4122 |
| $*P_{T_{sub-leading\ jet}}$ | 57 | 175 | 0 | 54 | 3.4122 |
| $not\ \mu^+\mu^-HZZ$ | 57 | 175 | 0 | 54 | 3.4122 |
| $not\ qqHZZ$ | 50 | 130 | 0 | 43 | 3.3773 |

Table 12: Remained backgrounds (more than 1 event) after all of cuts applied.

| name | scale | final |
|---|---|---|
| e2e2h_bb | 0.21896 | 8 |
| e2e2h_ww | 0.08176 | 7 |
| e3e3h_bb | 0.21784 | 2 |
| e3e3h_ww | 0.0812 | 9 |
| qqh_e3e3 | 0.4844 | 34 |
| qqh_ww | 1.6464 | 51 |
| qqh_zz | 0.20216 | 14 |
| zz_sl0mu_down | 1.08025726079 | 2 |
| zz_sl0tau_up | 1.10880522921 | 8 |
| zz_sl0tau_down | 1.10887174477 | 19 |
| ww_sl0muq | 1.10890944134 | 2 |
| ww_sl0tauq | 1.10899434445 | 3 |
| sze_l0mu | 1.10916641266 | 6 |

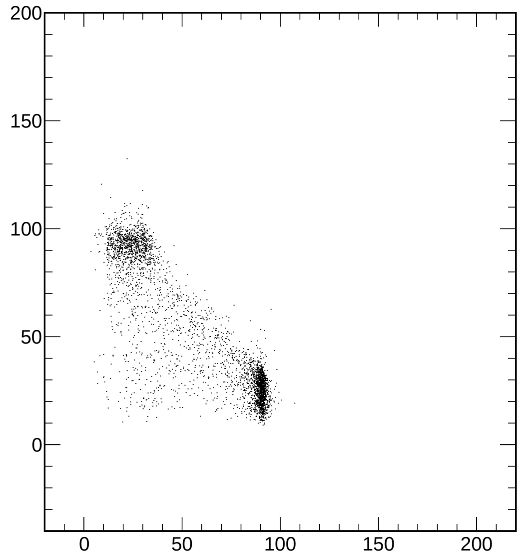


Figure 33: dimuon invariant mass vs dijet invariant mass.

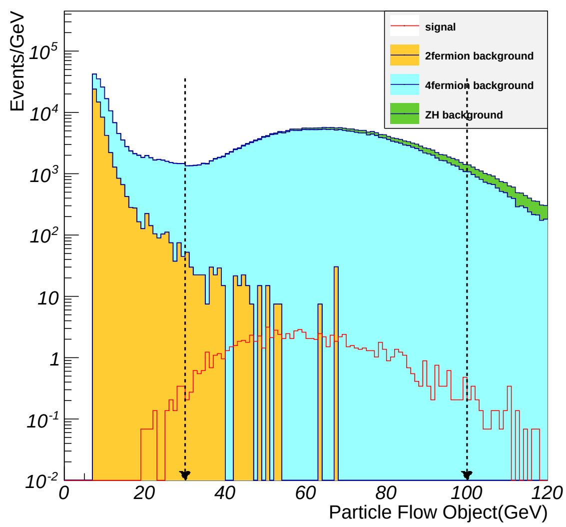


Figure 34: Number of PFOs.

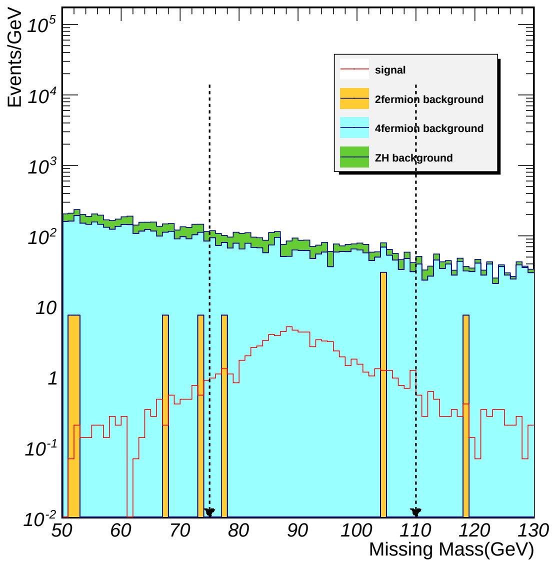


Figure 35: Recoil mass of visible particles.

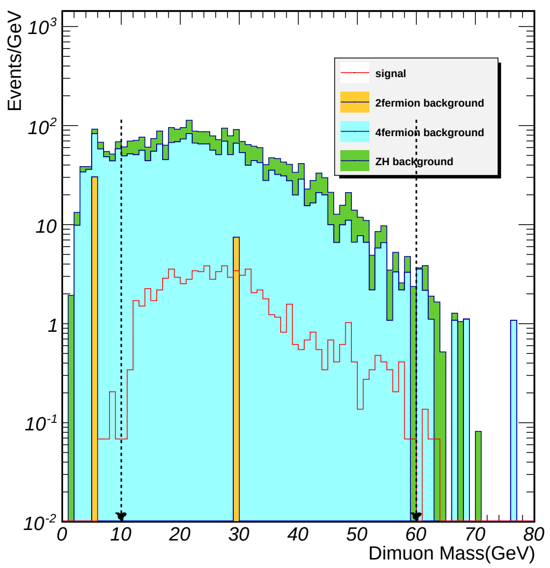


Figure 36: Invariant mass of di-muons.

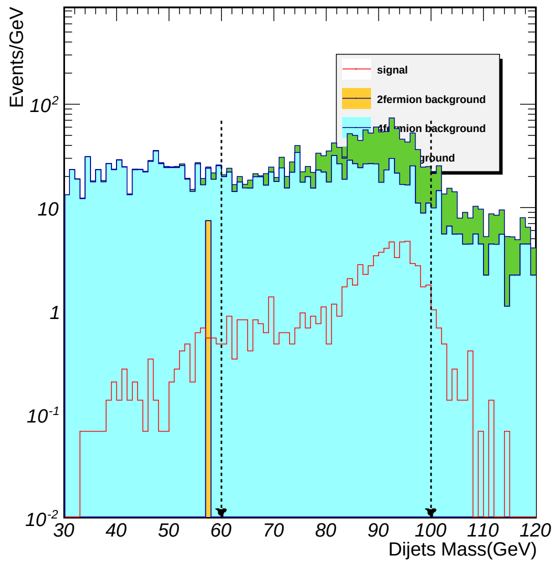


Figure 37: Invariant mass of di-jets.

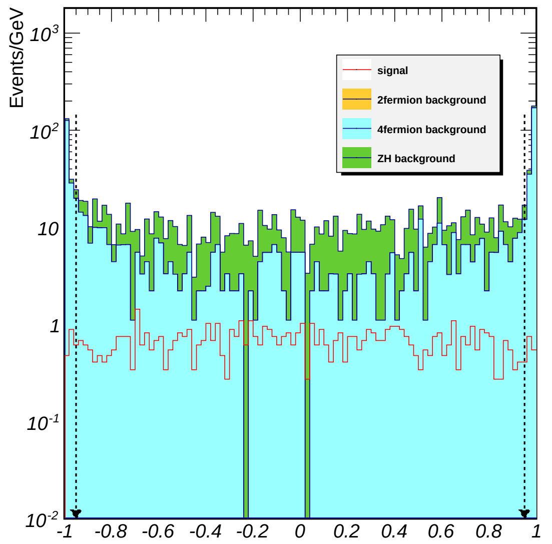


Figure 38: All visible particle $cos\ \theta$

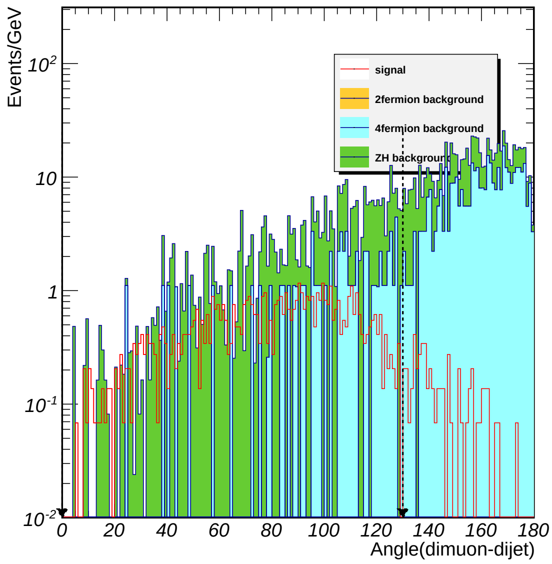


Figure 39: Minimum angle between the two Z(Z*) reconstructed by leptons and jets.

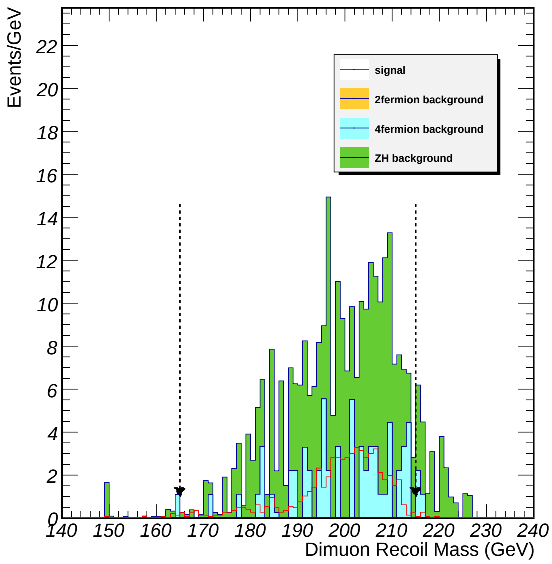


Figure 40: Recoil mass of dimuons.

- $Min\ angle < 130°$: Minimum angle between the two Z(Z*) reconstructed by leptons and jets should be within this range .

- $165GeV < M^{rec}_{dimuon} < 215GeV$ : the recoil mass of dimuons should be in this range.

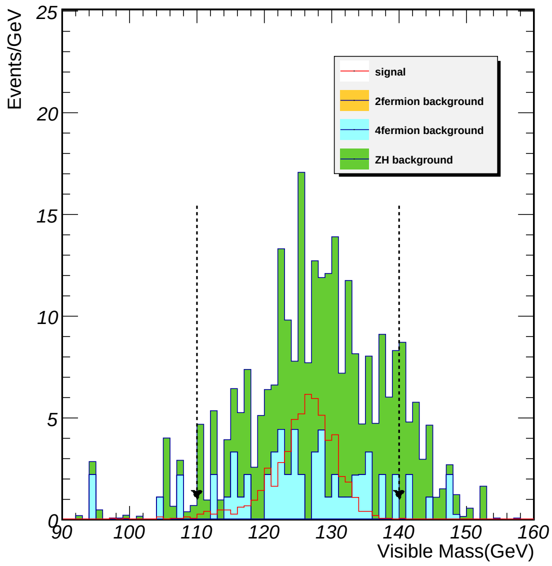


Figure 41: Invariant mass of all visible particles.

- $110GeV < M_{visible} < 140GeV$ : the invariant mass of all visible particles should be in this range.

Two additional cuts:

- $M^{rec}_{dimuon} < 122GeV\ or\ M^{rec}_{dimuon} > 128GeV$ : To avoid the overlap events with $\mu\mu$HZZ signals.

- $M^{rec}_{dijet} < 122GeV\ or\ M^{rec}_{dijet} > 128GeV$ : To remove the overlap events with $qq$HZZ signals.

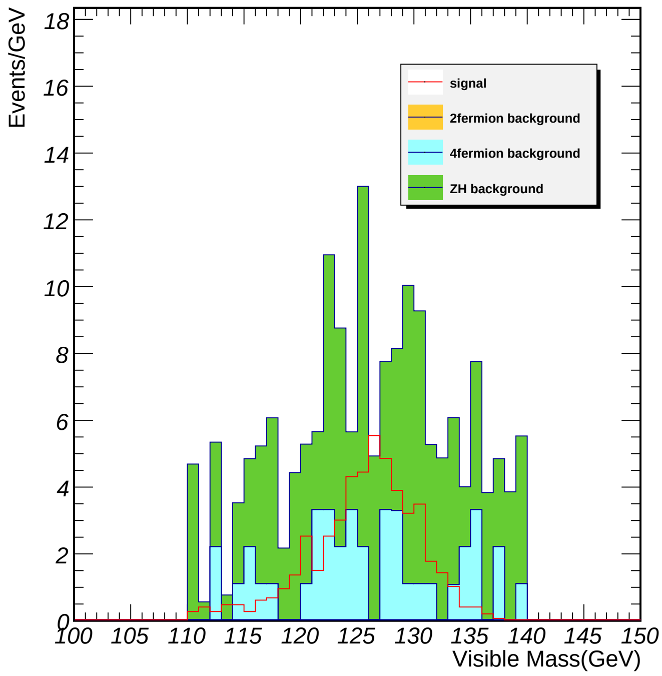


Figure 42: Distribution of the visible mass of all particles, after all of cuts applied.

# 6 Event Selection of Z($\rightarrow qq$)H(ZZ*$\rightarrow \nu\nu\mu\mu$)

## 6.1 Z($\rightarrow q\bar{q}$), H(Z$\rightarrow \nu\bar{\nu}$,Z*$\rightarrow \mu^+\mu^-$)

### 6.1.1 Event selection (Cut-based only)

Table 13: Cut flow table for $qq\nu\nu\mu\mu$ channel

| Cut | Signal | ZH background | 2f background | 4f background | $\frac{S}{\sqrt{S+B}}$ |
|---|---|---|---|---|---|
| $Expected$ | 20254 | 1140511 | 801811977 | 107203890 | |
| $Pre-selection$ | 826 | 30494 | 480828 | 515424 | |
| $Signal\ or\ not$ | 203 | 30291 | 480828 | 515424 | |
| $M_{missing} > M_{dimuon}$ | 94 | 3179 | 18606 | 40769 | 0.3795 |
| $N(pfo)$ | 84 | 2242 | 1212 | 12626 | 0.6659 |
| $M_{dijet}$ | 75 | 1532 | 7 | 4965 | 0.9263 |
| $M_{dimuon}$ | 68 | 1231 | 0 | 2803 | 1.0623 |
| $M_{missing}$ | 57 | 575 | 0 | 572 | 1.6625 |
| $*cos\ \theta$ | 57 | 575 | 0 | 572 | 1.6625 |
| $cos\theta_{visible}$ | 55 | 551 | 0 | 403 | 1.7334 |
| $*Angle_{\mu j}$ | 55 | 551 | 0 | 403 | 1.7334 |
| $M^{rec}_{dimuon}$ | 53 | 493 | 0 | 348 | 1.7877 |
| $M^{rec}_{dijet}$ | 51 | 418 | 0 | 237 | 1.9265 |
| $M_{visible}$ | 48 | 374 | 0 | 209 | 1.9087 |
| $*P_{visible}$ | 48 | 374 | 0 | 209 | 1.9087 |
| $*P_{T_{visible}}$ | 48 | 374 | 0 | 209 | 1.9087 |
| $*E_{leading\ jet}$ | 48 | 374 | 0 | 209 | 1.9087 |
| $*P_{T_{leading\ jet}}$ | 48 | 374 | 0 | 209 | 1.9087 |
| $*E_{sub-leading\ jet}$ | 48 | 374 | 0 | 209 | 1.9087 |
| $*P_{T_{sub-leading\ jet}}$ | 48 | 374 | 0 | 209 | 1.9087 |
| $not\ \mu^+\mu^-HZZ$ | 48 | 374 | 0 | 209 | 1.9087 |
| $not\ \nu\nu HZZ$ | 41 | 326 | 0 | 190 | 1.764 |

The event selection cuts are listed below in sequence.

- $M_{miss} > M_{dimuon}$ : the missing mass is greater than the dimuon invariant mass.

- $40 < N_{pfo} < 95$ : Number of Prticle Flow Objects should be in this range.

- $75GeV < M_{dijet} < 105GeV$ : the invariant mass of dijet should be in this range.

- $15GeV < M_{\mu^+\mu^-} < 55GeV$ : the invariant mass of the dimuon should be in this range.

Table 14: Remained backgrounds (more than 1 event) after all of cuts applied.

| name | scale | final |
|---|---|---|
| e2e2h_bb | 0.21896 | 14 |
| e2e2h_ww | 0.08176 | 4 |
| e3e3h_bb | 0.21784 | 9 |
| e3e3h_ww | 0.0812 | 11 |
| nnh_zz | 0.06832 | 34 |
| qqh_e3e3 | 0.4844 | 205 |
| qqh_ww | 1.6464 | 92 |
| zz_sl0mu_up | 1.09032214858 | 4 |
| zz_sl0mu_down | 1.08025726079 | 5 |
| zz_sl0tau_up | 1.10880522921 | 63 |
| zz_sl0tau_down | 1.10887174477 | 129 |
| sze_l0mu | 1.10916641266 | 6 |

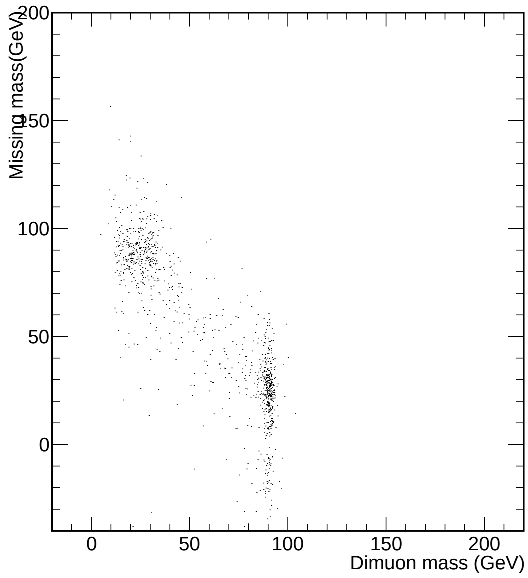


Figure 43: Missing mass vs dimuon invariant mass.

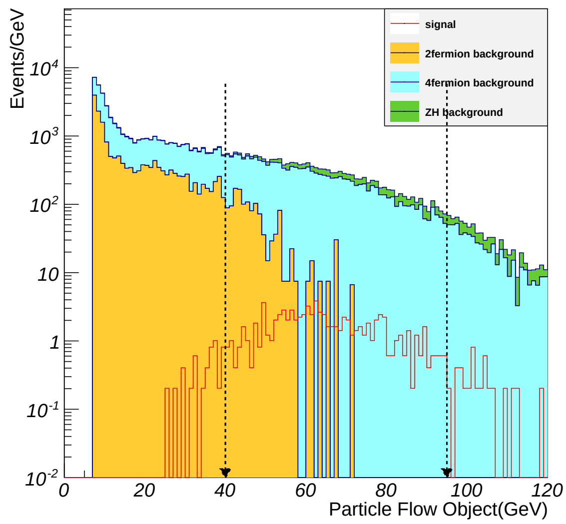


Figure 44: Number of PFOs.

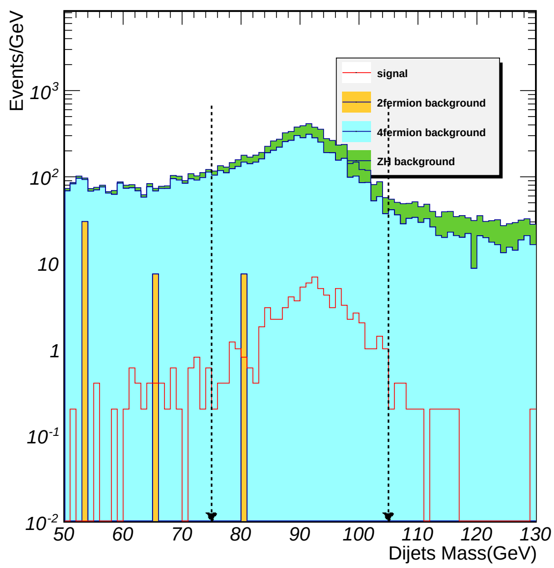


Figure 45: Invariant mass of di-jets.

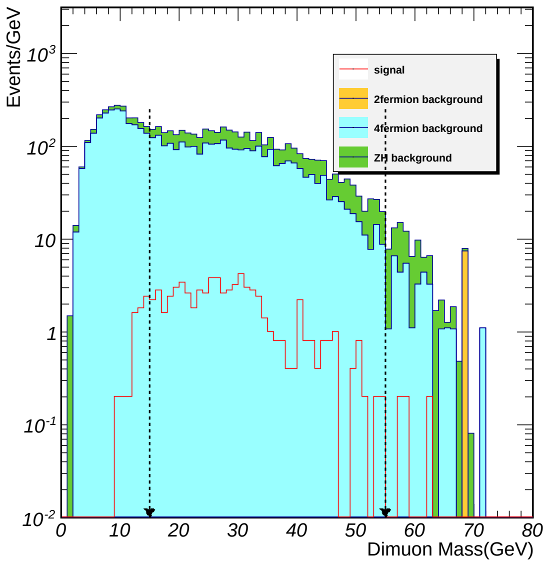


Figure 46: Invariant mass of di-muons.

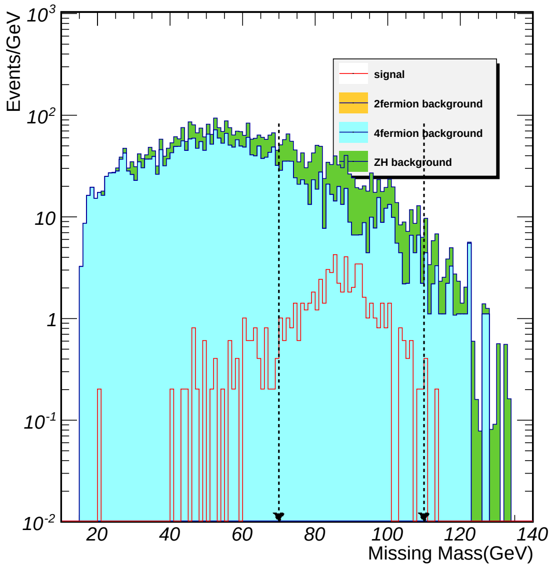


Figure 47: Recoil mass of visible particles.

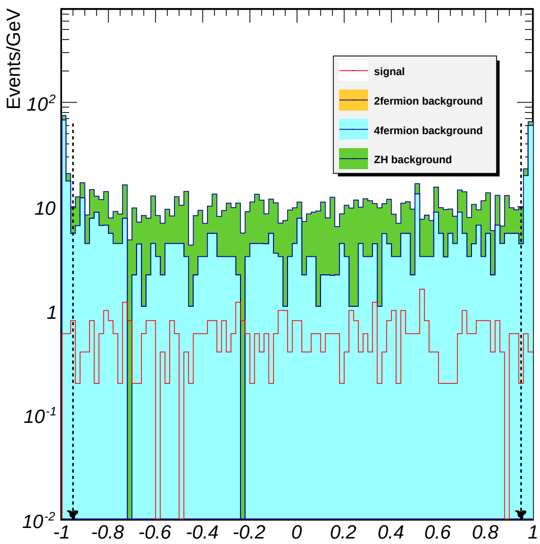


Figure 48: All visible particle $cos\ \theta$

- $70GeV < M^{Recoil}_{visible} < 110GeV$ : the recoil mass of all visible particles should be in this range.

- $-0.95 < cos_{plain} < 0.95$ : Cos calculated by all visible particle Pz and Py should be in this range

- $175GeV < M^{dimuon}_{Recoil} < 215GeV$: the recoil mass of the dimuon should be in this range.

- $110GeV < M^{dijet}_{Recoil} < 140GeV$: the recoil mass of the dijet should be in this range.

- $115GeV < M_{visible} < 155GeV$: the visible mass of all particles should be in this range.

Two additional cuts:

- $M^{rec}_{dimuon} < 122GeV\ or\ M^{rec}_{dimuon} > 128GeV$ : To avoid the overlap events with $\mu\mu$HZZ signals.
- $M_{visible} < 122GeV\ or\ M_{visible} > 128GeV$ : To remove the overlap events with $\nu\nu$HZZ signals.

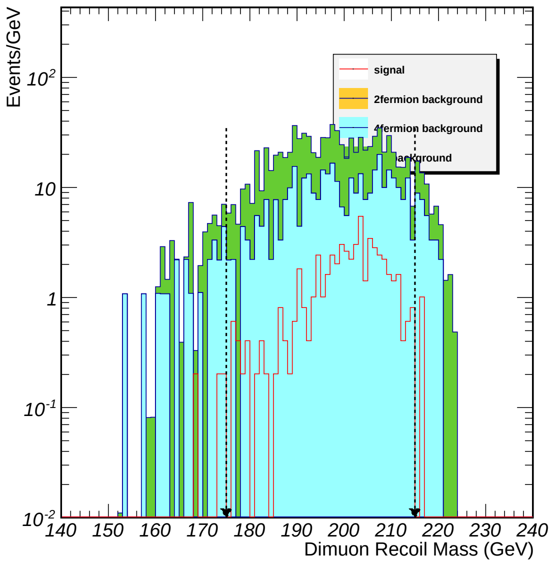


Figure 49: Recoil mass of di-muons.

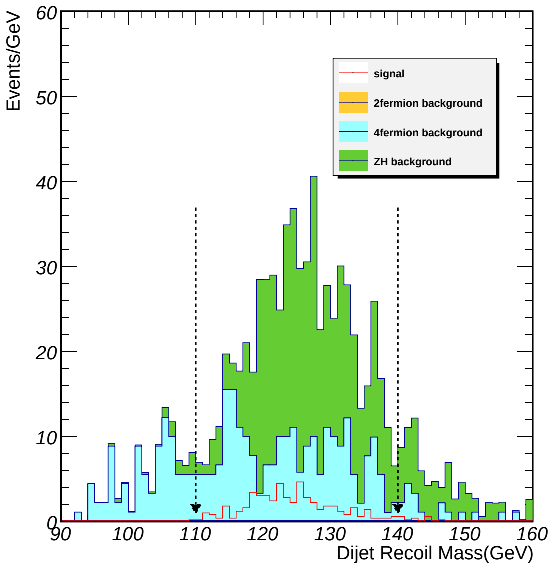


Figure 50: Recoil mass of di-jets.

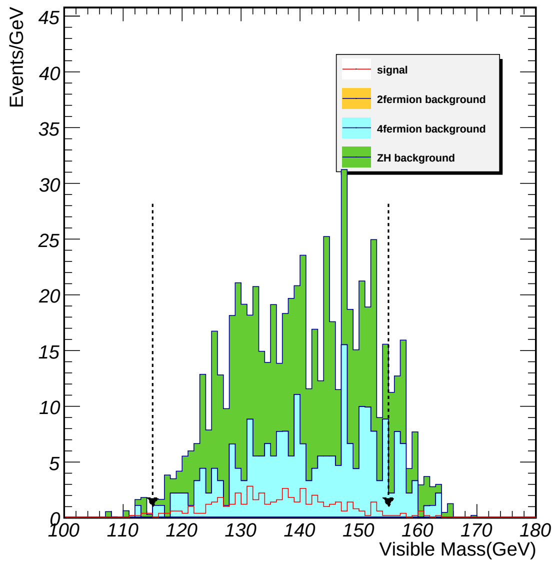


Figure 51: Visible mass of all particles.

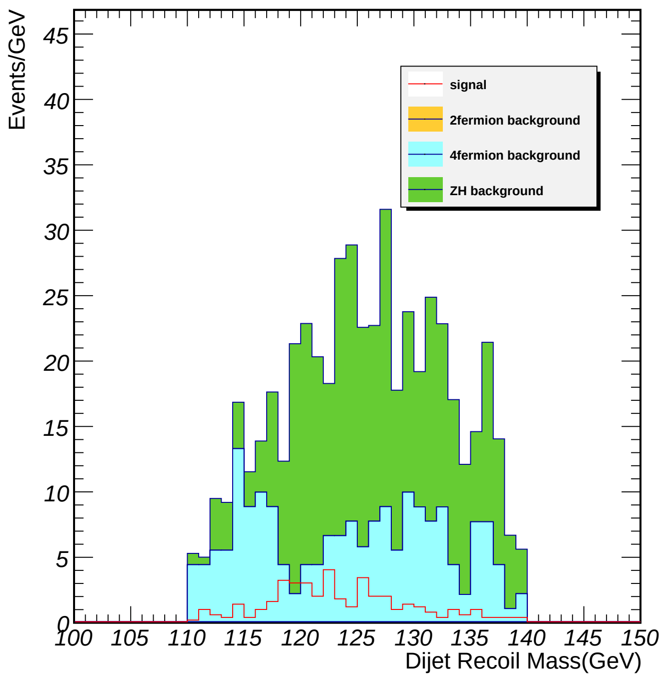


Figure 52: Distribution of the recoil mass of dijet, after all of cuts applied.

## 6.2 Z($\rightarrow q\bar{q}$), H(Z$\rightarrow\mu^+\mu^-$, Z*$\rightarrow\nu\bar{\nu}$)

### 6.2.1 Event selection (Cut-based only)

Table 15: Cut flow table for $qq\mu\mu\nu\nu$ channel

| Cut | Signal | ZH background | 2f background | 4f background | $\frac{S}{\sqrt{S+B}}$ |
|---|---|---|---|---|---|
| $Expected$ | 20254 | 1140511 | 801811977 | 107203890 | |
| $Pre-selection$ | 826 | 30494 | 480828 | 515424 | |
| $Signal\ or\ not$ | 203 | 30291 | 480828 | 515424 | |
| $M_{missing} < M_{dimuon}$ | 108 | 27112 | 462222 | 474655 | 0.1104 |
| $N(pfo)$ | 103 | 19806 | 17185 | 313602 | 0.1741 |
| $M_{dijet}$ | 97 | 4531 | 44 | 250527 | 0.1937 |
| $M_{dimuon}$ | 83 | 3468 | 14 | 174150 | 0.1989 |
| $M_{missing}$ | 64 | 1961 | 7 | 11132 | 0.5648 |
| $*cos\ \theta$ | 64 | 1961 | 7 | 11132 | 0.5648 |
| $cos\theta_{visible}$ | 60 | 1796 | 0 | 6827 | 0.652 |
| $Angle_{\mu j}$ | 53 | 1197 | 0 | 1264 | 1.0622 |
| $M^{rec}_{dimuon}$ | 51 | 1194 | 0 | 661 | 1.1737 |
| $M^{rec}_{dijet}$ | 48 | 950 | 0 | 534 | 1.2364 |
| $M_{visible}$ | 45 | 749 | 0 | 464 | 1.2781 |
| $*P_{visible}$ | 45 | 749 | 0 | 464 | 1.2781 |
| $*P_{T_{visible}}$ | 45 | 749 | 0 | 464 | 1.2781 |
| $*E_{leading\ jet}$ | 45 | 749 | 0 | 464 | 1.2781 |
| $*P_{T_{leading\ jet}}$ | 45 | 749 | 0 | 464 | 1.2781 |
| $*E_{sub-leading\ jet}$ | 45 | 749 | 0 | 464 | 1.2781 |
| $*P_{T_{sub-leading\ jet}}$ | 45 | 749 | 0 | 464 | 1.2781 |
| $not\ \mu^+\mu^- HZZ$ | 39 | 275 | 0 | 345 | 1.5366 |
| $not\ \nu\nu HZZ$ | 39 | 275 | 0 | 345 | 1.5366 |

The event selection cuts are listed below in sequence.

- $M_{miss} < M_{dimuon}$ : the dimuon invariantmass is greater than the missing mass.

- $35 < N_{pfo} < 100$ : Number of Prticle Flow Objects should be in this range.

- $75GeV < M_{dijet} < 110GeV$ : the invariant mass of dijet should be in this range.

- $75GeV < M_{\mu^+\mu^-} < 100GeV$ : the invariant mass of the dimuon should be in this range.

- $10GeV < M^{Recoil}_{visible} < 50GeV$ : the recoil mass of all visible particles should be in this range.

Table 16: Remained backgrounds (more than 1 event) after all of cuts applied.

| name | scale | final |
|---|---|---|
| e2e2h_bb | 0.21896 | 472 |
| e2e2h_cc | 0.011032 | 7 |
| e2e2h_e3e3 | 0.023968 | 1 |
| e2e2h_gg | 0.0326888819557 | 2 |
| e2e2h_ww | 0.08176 | 199 |
| e2e2h_zz | 0.010024 | 39 |
| e3e3h_zz | 0.009968099681 | 1 |
| qqh_e3e3 | 0.4844 | 18 |
| qqh_ww | 1.6464 | 3 |
| qqh_zz | 0.20216 | 2 |
| zz_sl0mu_up | 1.09032214858 | 135 |
| zz_sl0mu_down | 1.08025726079 | 324 |
| zz_sl0tau_up | 1.10880522921 | 2 |
| zz_sl0tau_down | 1.10887174477 | 2 |
| ww_sl0muq | 1.10890944134 | 1 |

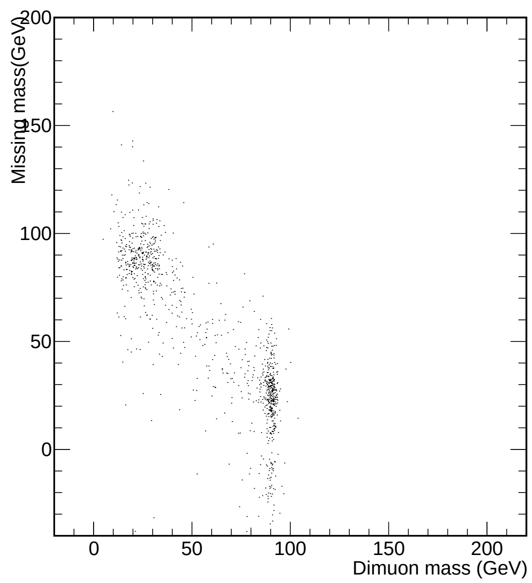


Figure 53: Missing mass vs dimuon invariant mass.

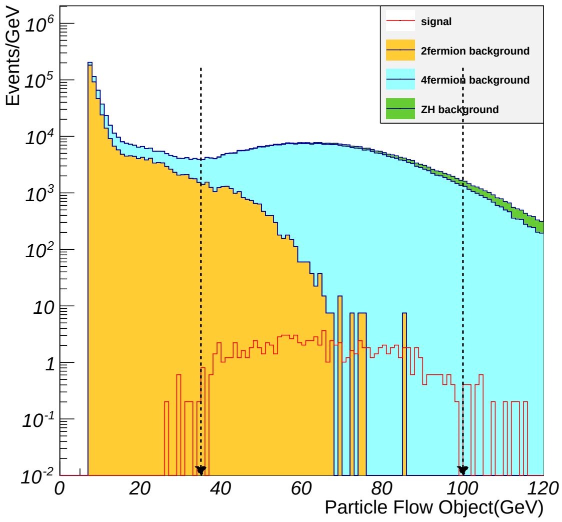


Figure 54: Number of PFOs.

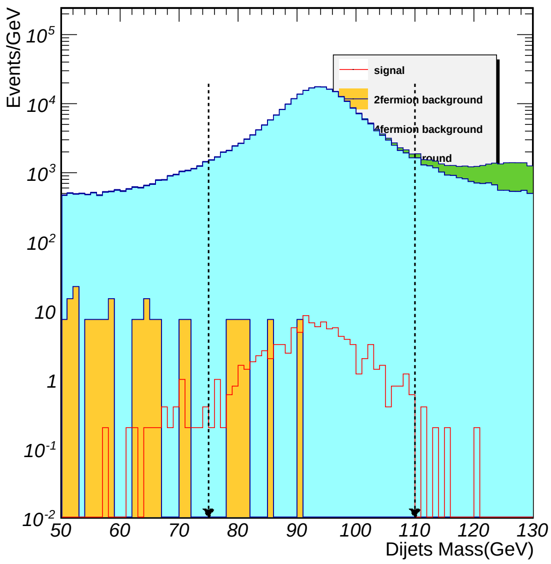


Figure 55: Invariant mass of di-jets.

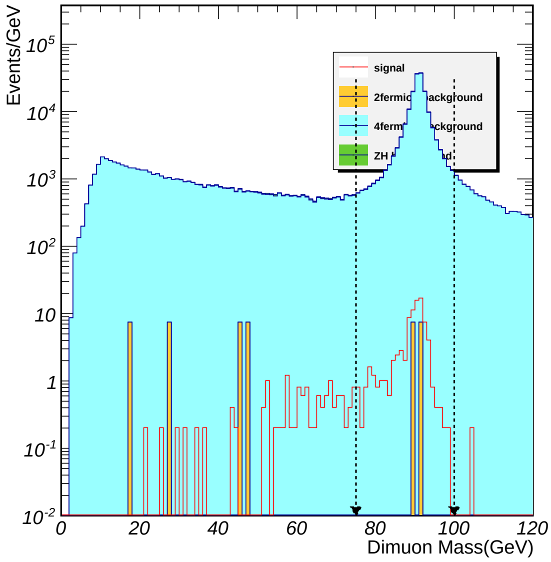


Figure 56: Invariant mass of di-muons.

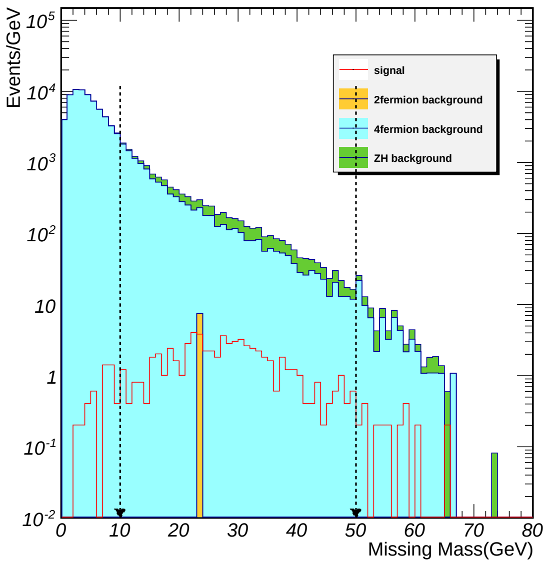


Figure 57: Recoil mass of visible particles.

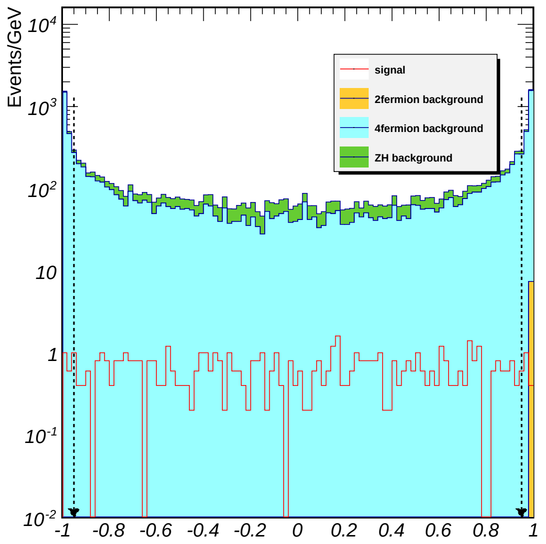


Figure 58: All visible particle $cos\ \theta$

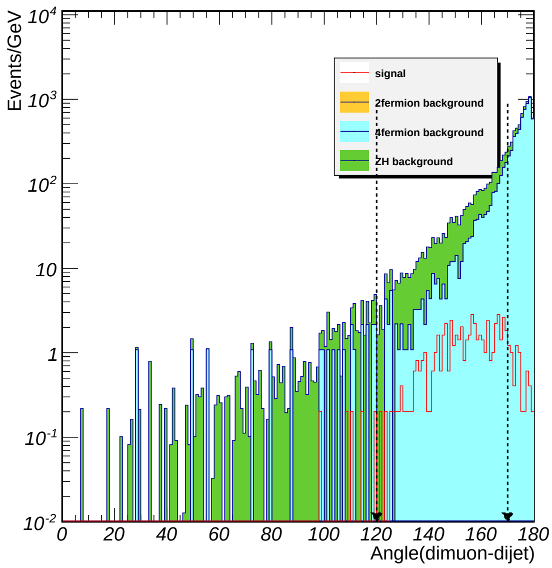


Figure 59: Minimum angle between the two Z(Z*) reconstructed by leptons and jets.

- $-0.95 < cos_{plain} < 0.95$ : Cos calculated by all visible particle Pz and Py should be in this range

- $120 < Min\ angle < 170°$: Minimum angle between the two Z(Z*) reconstructed by leptons and jets should be within this range .

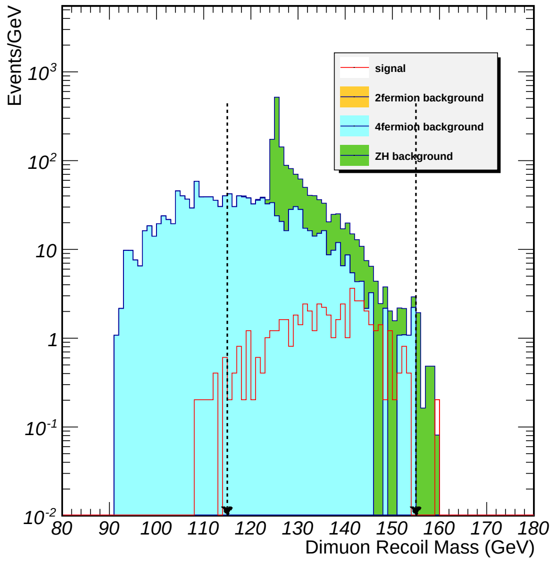


Figure 60: Recoil mass of di-muons.

- $115GeV < M^{dimuon}_{Recoil} < 155GeV$: the recoil mass of the dimuon should be in this range.

- $110GeV < M^{dijet}_{Recoil} < 140GeV$: the recoil mass of the dijet should be in this range.

- $185GeV < M_{visible} < 215GeV$: the visible mass of all particles should be in this range.

Two additional cuts:

- $M^{rec}_{dimuon} < 122GeV\ or\ M^{rec}_{dimuon} > 128GeV$ : To avoid the overlap events with $\mu\mu$HZZ signals.
- $M_{visible} < 122GeV\ or\ M_{visible} > 128GeV$ : To remove the overlap events with $\nu\nu$HZZ signals.

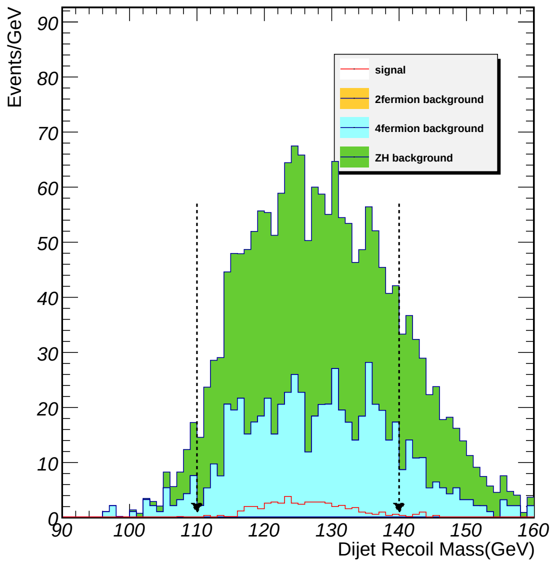


Figure 61: Recoil mass of di-jets.

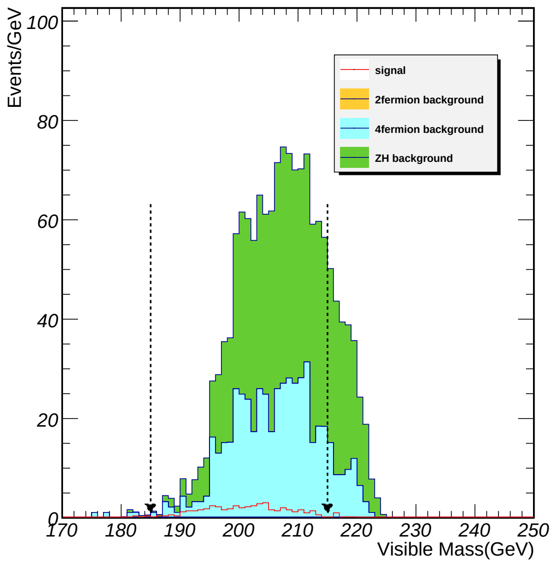


Figure 62: Visible mass of all particles.

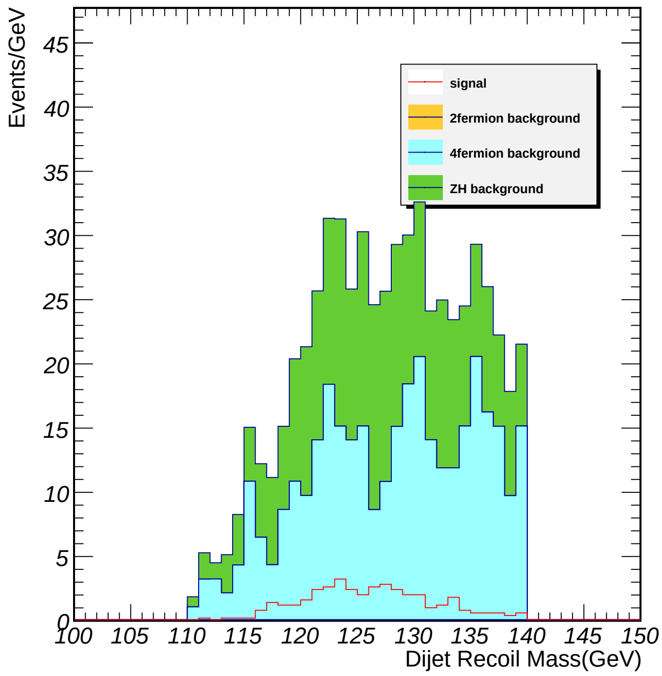


Figure 63: Distribution of the recoil mass of dijet, after all of cuts applied.

# 7 Result

## 7.1 Final Higgs mass distributions and fitting results.

### 7.1.1 $\mu\mu\nu\nu qq$ channel

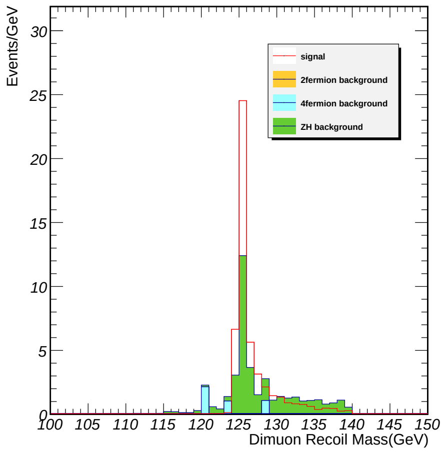


Figure 64: Final Higgs mass distribution of $\mu\mu\nu\nu qq$ (cut-based).

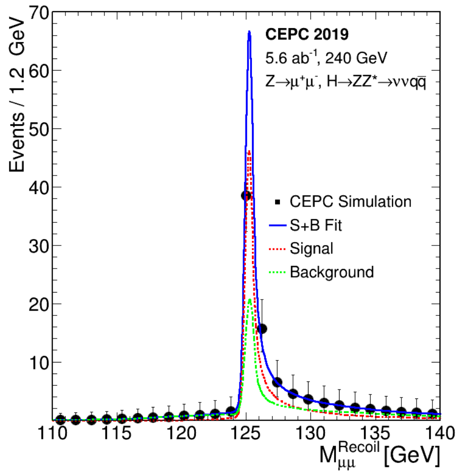


Figure 65: Fit result of $\mu\mu\nu\nu qq$ (cut-based).

### 7.1.2 $\mu\mu qq\nu\nu$ channel

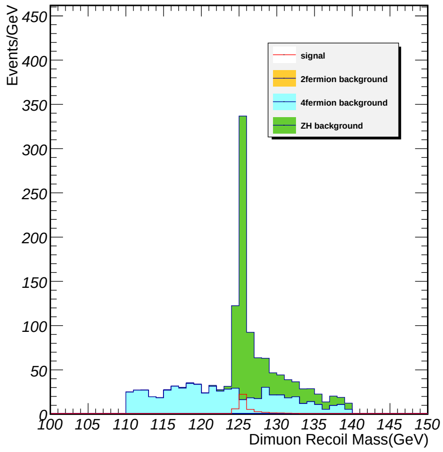


Figure 66: Final Higgs mass distribution of $\mu\mu qq\nu\nu$ (cut-based).

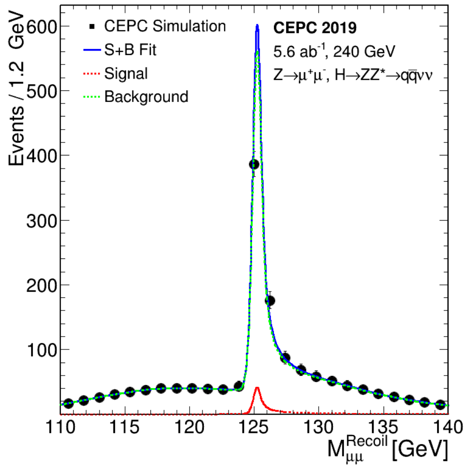


Figure 67: Fit result of $\mu\mu qq\nu\nu$ (cut-based).

### 7.1.3 $\nu\nu\mu\mu qq$ channel

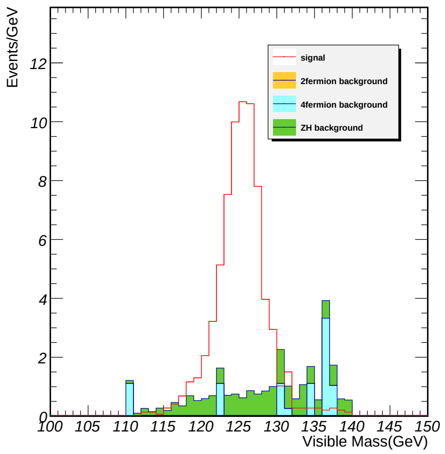


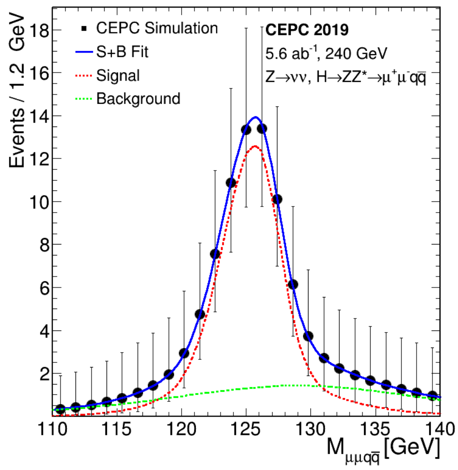


Figure 68: Final Higgs mass distribution of $\nu\nu\mu\mu qq$ (cut-based).

Figure 69: Fit result of $\nu\nu\mu\mu qq$ (cut-based).

#### 7.1.4 $\nu\nu qq\mu\mu$ channel

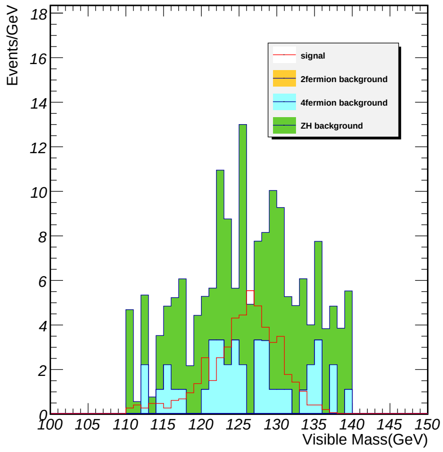


Figure 70: Final Higgs mass distribution of $\nu\nu qq\mu\mu$ (cut-based).

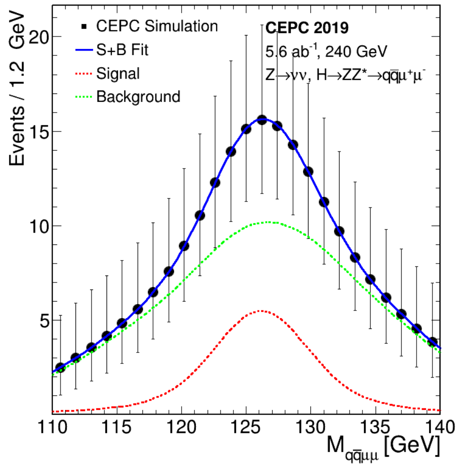


Figure 71: Fit result of $\nu\nu qq\mu\mu$ (cut-based).

### 7.1.5 $qq\mu\mu\nu\nu$ channel

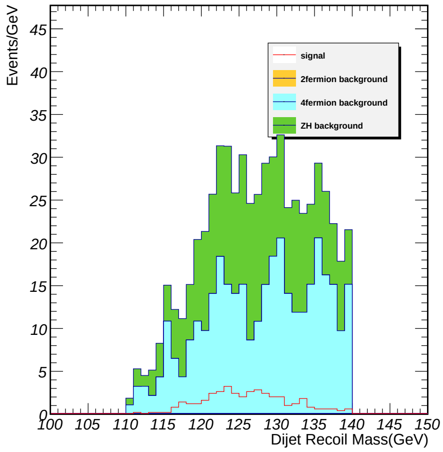


Figure 72: Final Higgs mass distribution of $qq\mu\mu\nu\nu$ (cut-based).

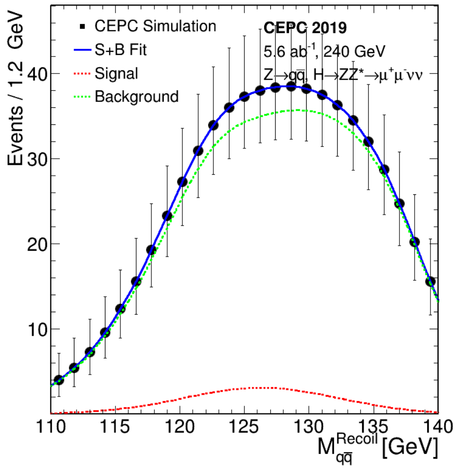


Figure 73: Fit result of $qq\mu\mu\nu\nu$ (cut-based).

259 ### 7.1.6 $qq\nu\nu\mu\mu$ channel

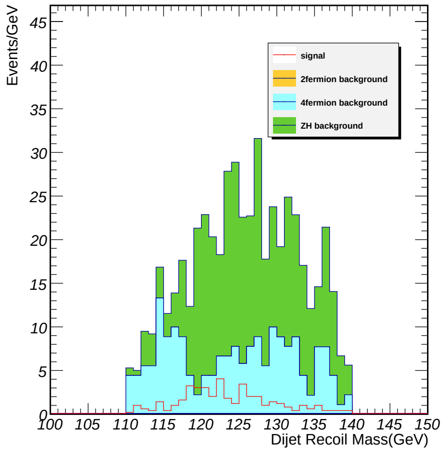


Figure 74: Final Higgs mass distribution of $qq\nu\nu\mu\mu$ (cut-based).

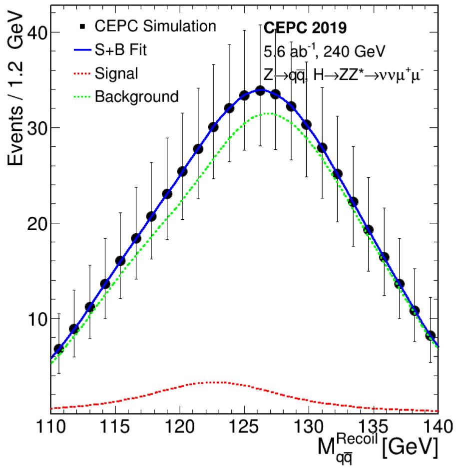


Figure 75: Fit result of $qq\nu\nu\mu\mu$ (cut-based).

## 7.2 *Calculations*

### 7.2.1 *Cut − based calculations*

According to the fit results,

$$precision\ of\ \sigma_{ZH} * BR_{signal} : \frac{\Delta\sigma_{ZH} * BR_{signal}}{\sigma_{ZH} * BR_{signal}}$$

is:

$$For\ \mu\mu\nu\nu qq : \ 18.146\%$$

$$For\ \mu\mu qq\nu\nu : \ 65.2495\%$$

$$For\ \nu\nu\mu\mu qq : \ 13.4518\%$$

$$For\ \nu\nu qq\mu\mu : \ 27.8294\%$$

$$For\ qq\mu\mu\nu\nu : \ 63.9272\%$$

$$For\ qq\nu\nu\mu\mu : \ 54.256\%$$

Branch ratio of Higgs to ZZ is

$$\frac{N_{signal}}{L\sigma_{ZH} Br_{Z\to\mu\mu} Br_{Z\to\nu\nu} Br_{Z\to jj}\epsilon}$$

Precision of Branch ratio of Higgs to ZZ is:

$$For\ \mu\mu\nu\nu qq : \ 18.146\%$$

$$For\ \mu\mu qq\nu\nu : \ 65.2495\%$$

$$For\ \nu\nu\mu\mu qq : \ 13.4518\%$$

$$For\ \nu\nu qq\mu\mu : \ 27.8294\%$$

$$For\ qq\mu\mu\nu\nu : \ 63.9272\%$$

$$For\ qq\nu\nu\mu\mu : \ 54.256\%$$

Combine results of Precision of Branch ratio of Higgs to ZZ is:

$$9.6762\%$$

Equations used for calculation of precision of Higgs width:

$$\Gamma_H = \frac{\Gamma_{H->ZZ^*}}{Br_{H->ZZ^*}} \propto \frac{\sigma_{ZH}}{Br_{H->ZZ^*}}$$

$$Precision\ of\ \Gamma_H : \frac{\Delta\Gamma_H}{\Gamma_H} = \sqrt{(\frac{\Delta\sigma_{ZH}}{\sigma_{ZH}})^2 + (\frac{\Delta Br_{H->ZZ^*}}{Br_{H->ZZ^*}})^2}$$

# References

[1] ATLAS Collaboration, Phys. Lett. B, **716**: 1-29 (2012), arXiv:1207.7214[hep-ex]

[2] CMS Collaboration, Phys. Lett. B, **716**: 30-61 (2012), arXiv:1207.7235[hep-ex]

[3] ATLAS Collaboration, Phys. Lett. B, **726**: 88-119 (2013), arXiv:1307.1427[hep-ex]

[4] ATLAS Collaboration, Phys. Lett. B, **726**: 120-144 (2013), arXiv:1307.1432[hep-ex]

[5] CMS Collaboration, JHEP, **1306**: 081 (2013), arXiv:1303.4571[hep-ex]

[6] CMS Collaboration, Nature Phys., **10**: (2014), arXiv:1401.6527[hep-ex]

[7] CMS Collaboration, Phys. Rev. D, **92**: 012004 (2015), arXiv:1411.3441[hep-ex]

[8] ATLAS and CMS Collaborations, JHEP, **08**: 045 (2016), arXiv:1606.02266[hep-ex]

[9] ATLAS and CMS Collaborations, Phys. Rev. Lett., **114**: 191803 (2015), arXiv:1503.07589[hep-ex]

[10] ATLAS Collaboration, Projections for measurements of Higgs boson signal strength and coupling parameters with the ATLAS detector at a HL-LHC, ATL-PHYS-PUB-2014-016 (2014) http://cds.cern.ch/record/1956710

[11] CMS Collaboration, Projected Performance of an Upgraded CMS Detector at the LHC and HL-LHC: Contribution to the Snowmass Process, arXiv:1307.7135[hep-ex]. http://www.slac.stanford.edu/econf/C1307292/docs/submittedArxivFiles/1307.7135.pdf